ACTA
FORESTALIA
FENNICA

Timo Kareinen, Ari Nissinen and Hannu Ilvesniemi

Analysis of Forest Soil Chemistry and Hydrology with a Dynamic Model ACIDIC

262 · 1998

ACTA FORESTALIA FENNICA

Publishers The Finnish Society of Forest Science
The Finnish Forest Research Institute

Editors Editor-in-chief Eeva Korpilahti
Production editors Seppo Oja, Tommi Salonen

Editorial Office Unioninkatu 40 A, FIN-00170 Helsinki, Finland
Phone +358 9 857 051, Fax +358 9 625 308, E-mail silva.fennica@metla.fi,
WWW http://www.metla.fi/publish/acta/

Aim and Scope Acta Forestalia Fennica publishes monographs in forest science. These may be original research articles or comprehensive reviews aiming at a synthesis of knowledge in a particular topic. The series covers all aspects of forest science, both basic and applied subjects. Manuscripts are subject to peer review.

ACTA FORESTALIA FENNICA

262 · 1998

Timo Kareinen, Ari Nissinen and Hannu Ilvesniemi

Analysis of Forest Soil Chemistry and Hydrology with a Dynamic Model ACIDIC

The Finnish Society of Forest Science — The Finnish Forest Research Institute

Kareinen, T., Nissinen, A. & Ilvesniemi, H. 1998. Analysis of forest soil chemistry and hydrology with a dynamic model ACIDIC. Acta Forestalia Fennica 262. 42 p.

In this study we analyze how the ion concentrations in forest soil solution are determined by hydrological and biogeochemical processes. A dynamic model ACIDIC was developed, including processes common to dynamic soil acidification models. The model treats up to eight interacting layers and simulates soil hydrology, transpiration, root water and nutrient uptake, cation exchange, dissolution and reactions of Al hydroxides in solution, and the formation of carbonic acid and its dissociation products. It includes also a possibility to a simultaneous use of preferential and matrix flow paths, enabling the throughfall water to enter the deeper soil layers in macropores without first reacting with the upper layers. Three different combinations of routing the throughfall water via macro- and micropores through the soil profile is presented. The large vertical gradient in the observed total charge was simulated succesfully. According to the simulations, gradient is mostly caused by differences in the intensity of water uptake, sulfate adsorption and organic anion retention at the various depths. The temporal variations in Ca and Mg concentrations were simulated fairly well in all soil layers. For H^+, Al and K there were much more variation in the observed than in the simulated concentrations. Flow in macropores is a possible explanation for the apparent disequilibrium of the cation exchange for H^+ and K, as the solution H^+ and K concentrations have great vertical gradients in soil. The amount of exchangeable H^+ increased in the O and E horizons and decreased in the Bs1 and Bs2 horizons, the net change in whole soil profile being a decrease. A large part of the decrease of the exchangeable H^+ in the illuvial B horizon was caused by sulfate adsorption. The model produces soil water amounts and solution ion concentrations which are comparable to the measured values, and it can be used in both hydrological and chemical studies of soils.

Keywords cation exchange, aluminium, macropores, micropores, leaching, simulation, modelling, water flow, flow paths.
Authors' address Department of Forest Ecology, P.O.Box 24, 00014 University of Helsinki, Finland.
Telefax +358-9-191 7605
E-mail hannu.ilvesniemi@helsinki.fi; timo.kareinen@helsinki.fi; ari.nissinen@helsinki.fi.
Accepted 22 December 1998.

ISBN 951-40-1663-7
ISSN 0001-5636
Tampere 1998, Tammer-Paino Oy

Contents

List of symbols, variables and parameters 4
1 INTRODUCTION 7
2 MODEL THEORY AND FORMULATIONS 8
2.1 General 8
2.2 Hydrological processes 10
2.2.1 Precipitation and ion deposition 10
2.2.2 Vertical water flow in micropores 10
2.2.3 Vertical water flow in macropores 12
2.2.4 Water flow between macro- and micropores 12
2.2.5 Infiltration 13
2.2.6 Horisontal outflow 13
2.2.7 Surface water flow 13
2.2.8 Transpiration 13
2.2.9 Plant water uptake 14
2.3 Tree growth 14
2.3.1 Growth 14
2.3.2 Nutrient uptake 14
2.4 Soil chemical processes 15
2.4.1 Water autoprotolysis 15
2.4.2 Carbon dioxide dissolution and carbonic acid dissociation 15
2.4.3 Hydrolysis of aluminum compounds and aluminum complexation with sulfate 16
2.4.4 Mineral solubility 16
2.4.5 Cation exchange 17
2.4.6 Sulfate adsorption 17
2.4.7 Formation and precipitation of organic complexes 18
2.4.8 Weathering 18
3 APPLICATION OF THE MODEL TO RUDBÄCKEN 19
3.1 General 19
3.2 Simulated cases 19
3.3 Site description, experimental design and chemical analyses 20
3.4 Model inputs and parameter values 20
4 RESULTS AND DISCUSSION 23
4.1 Soil water content 23
4.2 Water flow routes 25
4.3 Total charge of the soil solutions 26
4.4 Effects of different hydrological descriptions on simulated total charge 28
4.5 Cation concentrations in the soil solutions 32
4.5.1 Ca and Mg 32
4.5.2 H^+, Al and K 34
4.6 Changes in exchangeable cations 35
4.7 The use of model ACIDIC for analysis of deposition effects 37
5 CONCLUSIONS 39
Acknowledgements 39
REFERENCES 40

List of Symbols, Variables and Parameters

Common symbols

θ = water content of soil [l (water) l^{-1} (total volume)]
ρ = density [kg m^{-3}]
A = area [m^2] or area index [m^2 m^{-2}]
d = diameter [m]
h = water potential (hydraulic head) [m]
I,J = ions
$[I]$ = concentration of ion I dissolved [mol l^{-1}] or adsorbed [mol kg^{-1}]
K = hydraulic conductivity [mm s^{-1}]
m = mass [kg m^{-2}]
n = number of soil layers or number of a spesific soil layer
q = water flux [l m^{-2} s^{-1}]
S = saturation of storage
t = length of season [days]
T = temperature [°C]
W = amount of water [l m^{-2}]
x = (horisontal) distance [m]
z = (vertical) distance from top of the soil [m]
Z = charge of ion [mol_c mol^{-1}]

Subscripts

subscript $_a$ = adsorbed phase variable
subscript $_c$ = micropore variable
subscript $_e$ = variable reflects to effective volume
subscript $_g$ = macropore variable
subscript $_{gc}$ = variable reflects to the water flow between macro- and micropores
subscript $_i$ = variable of soil layer i
subscript $_s$ = water saturated phase variable
subscript $_r$ = dry phase variable (only a residual amount of water exists)
subscript $_{CE}$ = cation echange variable
subscript $_I$ = variable of ion I
subscript $_L$ = leaf variable
subscript $_M$ = mineral variable
subscript $_{MW}$ = mineral weathering variable
subscript $_P$ = precipitation variable
subscript $_R$ = root variable
subscript $_S$ = soil variable
subscript $_{SA}$ = sulfate adsorption variable
subscript $_{SS}$ = soil surface variable
subscript $_T$ = plant or tree variable
subscript $_{TG}$ = tree growth variable
subscript $_{NU}$ = nutrient uptake variable

System definition variables

β = average slope angle of the examined site [°]
ρ_{BD} = soil bulk density [kg m^{-3}]
ρ_R = (fine)root density[kg m^{-3}]
d_g = macropore diameter [m]
d_R = fineroot diameter [m]
$[I_T]$ = concentration of ion I in tree stems [mol kg^{-1}]
$[I_M]$ = concentration of ion I in minerals [mol kg^{-1}]
L_R = ratio of root lenght to root mass [m kg^{-1}]
n_S = number of soil layers in simulation
z_S = thickness of soil layer [m]

State variables

θ_c = water content of micropores [l l^{-1}]
θ_g = water content of macropores [l l^{-1}]
θ_T = water content of plant water storage [l l^{-1}]
A_g = area index of macropore walls [m^2 m^{-2}]
A_L = leaf area index [m^2 m^{-2}]
A_R = root area index [m^2 m^{-2}]
e_s = saturated water vapour [g m^{-3}]
h_c = water potential of micropores [m]
h_T = water potential of plant water storage [m]
$[I_a]$ = concentration of adsorbed ion I [mol kg^{-1}]
$[I_c]$ = concentration of ion I in micropore water [mol l^{-1}]
$[I_g]$ = concentration of ion I in macropore water [mol l^{-1}]
K_c = hydraulic conductivity of micropores [mm s^{-1}]

m_T = tree stem biomass [kg m^{-2}]
p_{CO_2} = CO_2 partial pressure [%]
S_g = macropore saturation
S_T = saturation of plant water storage
S_{ec} = effective saturation of micropores
T = actual air temperature [°C]
T_{mean} = mean day air temperature [°C]
v_{NUI} = uptake rate of ion I [l m^{-2} s^{-1}]
W_c = water amount in micropores [l m^{-2}]
W_g = water amount in macropores [l m^{-2}]
W_{SS} = water amount in soil surface [l m^{-2}]
W_T = water amount in plant water storage [l m^{-2}]
z = distance of soil layer midpoint from the soil surface [m]
z_S = soil layer thickness [m]

Flow variables

C_{alun} = mass flow of ions in precipitation/dissolution of alunite [mol l^{-1} s^{-1}]
C_{gibb} = mass flow of ions in precipitation/dissolution of gibbsite [mol l^{-1} s^{-1}]
C_{gyps} = mass flow of ions in precipitation/dissolution of gypsum [mol l^{-1} s^{-1}]
C_{kaol} = mass flow of ions in precipitation/dissolution of kaolinite [mol l^{-1} s^{-1}]
C_{AlOH} = mass flow of ions in hydrolysis of Al^{3+} to $AlOH^{2+}$ [mol l^{-1} s^{-1}]
$C_{Al(OH)_2}$ = mass flow of ions in hydrolysis of Al^{3+} to $Al(OH)_2^+$ [mol l^{-1} s^{-1}]
$C_{Al(OH)_3}$ = mass flow of ions in hydrolysis of Al^{3+} to $Al(OH)_3$ [mol l^{-1} s^{-1}]
C_{AlS} = mass flow of ions in complexation of Al^{3+} with SO_4^{2-} [mol l^{-1} s^{-1}]
C_{CO} = mass flow of ions in carbon dioxide dissolution [mol l^{-1} s^{-1}]
C_{CA} = mass flow of ions in carbonic acid dissociation [mol l^{-1} s^{-1}]
C_{H_2O} = mass flow of ions in water autoprotolysis [mol l^{-1} s^{-1}]
CE_{I-J} = mass flow of ions in cation exchange between ions I and J [mol l^{-1} s^{-1}]
IF_c = infiltration to micropores [l m^{-2} s^{-1}]
IF_g = infiltration to macropores [l m^{-2} s^{-1}]
MW = mineral weathering [mol m^{-2} s^{-1}]
NU_I = uptake of ion I by tree stems [mol m^{-2} s^{-1}]
OC = mass flow of ions in precipitation of organic complexes [mol l^{-1} s^{-1}]
P = precipitation [l m^{-2} s^{-1}]
q_c = vertical water flow in micropores [l m^{-2} s^{-1}]
q_g = vertical water flow in macropores [l m^{-2} s^{-1}]
q_{gc} = water flow from macropores to micropores [l m^{-2} s^{-1}]
q_{gg} = water outflow from macropores [l m^{-2} s^{-1}]
q_T = water uptake by tree stems [l m^{-2} s^{-1}]
SA = mass flow of ions in sulfate adsorbtion [l m^{-2} s^{-1}]
SF = surface flow [l m^{-2} s^{-1}]
TG = tree stem growth [kg m^{-2} s^{-1}]
TR = transpiration [l m^{-2} s^{-1}]

Weather and deposition variables

$[I_P]$ = concentration of ion I in precipitation [mol l^{-1}]
T_{max} = maximum day air temperature [°C]
T_{min} = minimum day air temperature [°C]
W_P = daily rainfall [l m^{-2}]

Process parametres

α = parameter of Van Genuchten's equation for soil water retention curve
θ_{sc} = saturated water content of micropores [l l^{-1}]
θ_{sg} = saturated water content of macropores [l l^{-1}]
θ_{sT} = saturated water content of tree stems [l l^{-1}]
θ_{rc} = residual water content of micropores [l l^{-1}]
A_{plot} = area of the plot [m^2]
h_{gc} = treshold water potential in water flow between macro- and micropores [m]
k_{alun} = equilibrium coefficient of alunite solubility
k_{gibb} = equilibrium coefficient of gibbsite solubility
k_{gyps} = equilibrium coefficient of gypsum solubility
k_{kaol} = equilibrium coefficient of kaolinite solubility
k_{AlOH} = equilibrium coefficient of hydrolysis of Al^{3+} to $AlOH^{2+}$
$k_{Al(OH)_2}$ = equilibrium coefficient of hydrolysis of Al^{3+} to $Al(OH)_2^+$
$k_{Al(OH)_3}$ = equilibrium coefficient of hydrolysis of Al^{3+} to $Al(OH)_3$
k_{AlSO_4} = equilibrium coefficient of complexation of Al^{3+} with SO_4^{2-}
k_{I-J} = equilibrium coefficient of cation exchange reaction between ions I and J
k_{CO} = equilibrium coefficient of carbon dioxide dissolution
k_{CA} = equilibrium coefficient of carbonic acid dissociation

k_{H2O}= equilibrium coefficient of water autoprotolysis
k_{SA} = equilibrium coefficient of sulfate adsorption [mol l^{-1}]
K_{sc} = saturated hydraulic conductivity of micropores [mm s^{-1}]
K_{sg} = saturated hydraulic conductivity of macropores [mm s^{-1}]
K_L = conductance of leaf stomatas [mm s^{-1}]
l = parameter of Mualem's equation (water content – conductivity)
n = parameter of Van Genuchten's equation for soil water retention curve
m = parameter of Van Genuchten's equation for soil water retention curve
pCO_{2win} = CO_2 partial pressure in winter [%]
pCO^2_{spr} = maximum CO_2 partial pressure in spring [%]
pCO_{2sum} = CO_2 partial pressure in summer [%]
pCO_{2aut} = maximum CO_2 partial pressure in autumn [%]
R_{am} = morning fraction of daily rainfall [%]
R_I = rain intensity [mm s^{-1}]
t_{aut} = length of autumn [julian days]
t_{spr} = length of spring [julian days]
t_{sum} = length of summer[julian days]
t_{win} = length of winter[julian days]
T_{TG} = threshold growth temperature [°C]
v_{TG} = rate coefficient of tree stem growth [kg m^{-2} s^{-1}]
v_{MW} = rate coefficient of mineral weathering [kg m^{-2} s^{-1}]
x_{cR} = average distance between midpoints of the micropore and root channels [m]
x_{gc} = average distance between midpoints of the macro- and micropore channels [m]
x_{plot} = average distance between midpoint and border of the plot [m]
z_{SS} = threshold height of surface water pool [m]
$[(SO_4)_{a-max}]$ = maximum sulfate adsorption capacity of the soil [mol kg^{-1}]

1 Introduction

Changes in the soil chemical characteristics induced by changes in the deposition have been under extensive research over the last two decades. Important empirical background for the hypothesis of soil acidification has been obtained from comparisons of the soil samples collected from the same location previously and again at the present day. However, the quantification of the changes by the means of historical documentation has been problematic because of the difficulties in distinguishing between different causes in the change detected (Falkengren-Grerup et al. 1987, Tamm and Hallbäcken 1988). Further, extrapolating any results of experimental acidification studies to other geomorphological areas is difficult, because of widely divergent soil properties. Forest-wide experiments are expensive and may take decades before results are obtained, if realistic inputs of acid deposition are used. For these reasons a lot of work concerning the effects of acid load on soil nutrient leaching and aluminium solubility has been done by using mathematical models which combine the ecosystem element fluxes with the theoretical and experimental knowledge of soil chemistry.

Model structure and selection of processes to be considered should always be related to the aim of the study. In acidification analysis description of cation exchange and aluminium solubility have formed the core of the models (see e.g. Cosby et al. 1985). Major simplifying assumptions have been made regarding vertical soil heterogenity, plant nutrient uptake and decomposition of soil organic matter, and water flow paths (see e.g. Jenkins and Cosby 1989, Tiktak and Van Grinsven 1995).

Most of the biological activity modifying and responding to the chemical conditions and processes in soils is located in the upper soil horizons. Thus, the main interest in the effects of the acidic deposition or climate change on soils and tree growth concerns the reactions of the uppermost part of the pedon. In boreal coniferous forests soluble organic compounds dissolve aluminium and iron compounds in the upper mineral soil. This podzolisation process leads to transportation of sesquioxides and organic compounds down the profile, and to precipitation of these compounds deeper in the soil. The soil chemical properties, solution ion composition and soil waterholding capacity vary greatly between the horizons within a soil (Nissinen et al. 1998, Mecke et al. 1999). Thus, in models dealing with forest soils, especially podzols, the division of the model description into different soil horizons has to be considered.

Major soil chemical reactions and the transport of different compounds take place in the water surrounding the soil matrix. The flow paths of the soil solution determine the proportion of water, which react chemically with the different soil horizons or with particle surfaces in pores of different sizes. A fraction of the soil solution can flow out of the system in the macropores and avoid contact with the chemically reactive surfaces of small pores and soil particles (Bewen et al. 1982, Luxmoore et al. 1990). A realistic description of the soil hydrology is thus important for the proper model output, although data on the actual amount of rapid macropore flow in soils is scarce. In addition, the ability to simulate hydrology and water flow paths enables analysis of the effects of the hydrological changes generated by climate change on ecosystems.

In this study we analyze how the ion concentrations in forest soil solution are determined by hydrological and biogeochemical processes. Special attention was paid on the effect of preferential flow in macropores on soil solution chemistry. A dynamic model (ACIDIC, Analysis of Climate Change Impact and Deposition Impact on Soil Chemistry) was developed for this purpose and is described here. The model behaviour is tested by comparing simulated ion concentrations to observed ones in the horizons of a podzolic forest soil.

2 Model Theory and Formulations

2.1. General

A large number of biogeochemical reactions associated with carbon, nitrogen, sulfur and base cation cycles determine the hydrogen ion cycle of a forest ecosystem, which must be considered in analyzing the soil acidification phenomenon (Ulrich 1983, De Vries and Breeuwsma 1987). Biological processes – plant growth, nutrient uptake, litter production and decomposition of soil organic matter – play major roles in these cycles. Water flow is an important process, convecting ions into and out of the soil.

Looking at the amounts of various cations in the soil solution, the processes can be divided to two categories: those affecting the proportions of the various cations in the solution, and those affecting the total amount of cations and anions in the solution (Johnson and Cole 1980). In addition, evapotranspiration increases ion concentrations by decreasing the quantitity of water, in which the ions are dissolved.

The chemical reactions that determine the proportions of cations in the soil solution are cation exchange and dissolution of aluminium compounds and minerals. The exchangeable cations act as a buffer against rapid changes in cation concentrations, because the quantity of each exchangeable cation species on exchange sites is much larger than in solution. The main ions involved in the exchange processes are Ca^{2+}, Mg^{2+}, K^+, Na^+, Al^{3+} and H^+, the proportions of these being different in the various soil layers. The reactions of aluminium are particularly complicated, since the amounts of Al in soil solution are also affected by chelation with dissolved organic ions and the solubility of inorganic and organic aluminium compounds, which depend on solution acidity.

The proportions of cations in the soil solution are also affected by the cation uptake of plants, which produces the same amount (mol_c) of protons in the solution as base cations and ammonium are taken up. Correspondingly, weathering of minerals and decomposition of organic matter produce base cations in the solution and consume protons from the solution.

The total amount of cations and anions in the soil solution is affected by the transport of ions in and out of the soil system (i.e. deposition and leaching). In addition, it is affected by the dissolution and retention of specific anions and accompanying cations (Johnson and Cole 1980, De Vries and Breeuwsma 1987). Nitrate may be taken up by plants and microbes (see e.g. Mengel and Kirkby 1987). Change in both anion and cation concentrations results. Sulfate adsorption and precipitation also consumes H^+ from the soil solution.

The dissolution and dissociation of organic anions increases the solution cation and anion concentrations in the topsoil, whereas deeper in the soil, a major part of the organic anions precipitate with metals, reducing the ionic strength of the solution. Also the soil solution pH is regulated by the organic acids.

The biological processes – root growth, nutrient uptake, and decomposition of soil organic matter – consume energy bound to the carbohydrates, carbon being released in the form of CO_2 in respiration. The CO_2 reacts with water, forming carbonic acid and further bicarbonate, and affects the anion and cation concentrations in solution. The production of CO_2 in a soil being the result of biological processes, it is affected by soil moisture, temperature and chemical conditions. The CO_2 concentration in the air in the soil is also determined by the diffusion rate, which is a function of the air-filled pore-space.

Most of the processes and reactions described above have been included in ACIDIC. However, compared to the general theory, the definition of a mathematical description of the system has required a more rigid formulation of the processes. In the following some major assumptions are introduced, clarifying also some general aspects of the model structure:

1) Soil is divided into layers. Layers can differ from each other in respect of all properties defined, but within each layer the properties are homogenous.
2) The difference in the water potential between the layers is the driving force of the water flow. A rapid preferential flow in macropores may also be simulated, but chemical and biological processes affect ion concentrations in micropores only. Between the macro- and micropores ions are transported by water flow. The same holds for the ion transport between the layers. Diffusion of ions is not taken into account.
3) Plant growth is equal to tree growth, which is not affected by the soil properties. Tree growth is described as stem growth regulated by the air temperature. The uptake of nutrients is calculated from ions needed for stem growth, and the uptake for the growth of needles, branches and roots is assumed to be equal to the release in the decomposition of soil organic matter.
4) The vertical distribution of nutrient uptake is based on amounts of roots and nutrient concentrations in each soil layer.
5) Transpiration is linked with the soil moisture. This is done by describing a plant water storage and assuming a relationship between the saturation of the storage and water potential of the plant. Simulated transpiration decreases with decreasing satu-

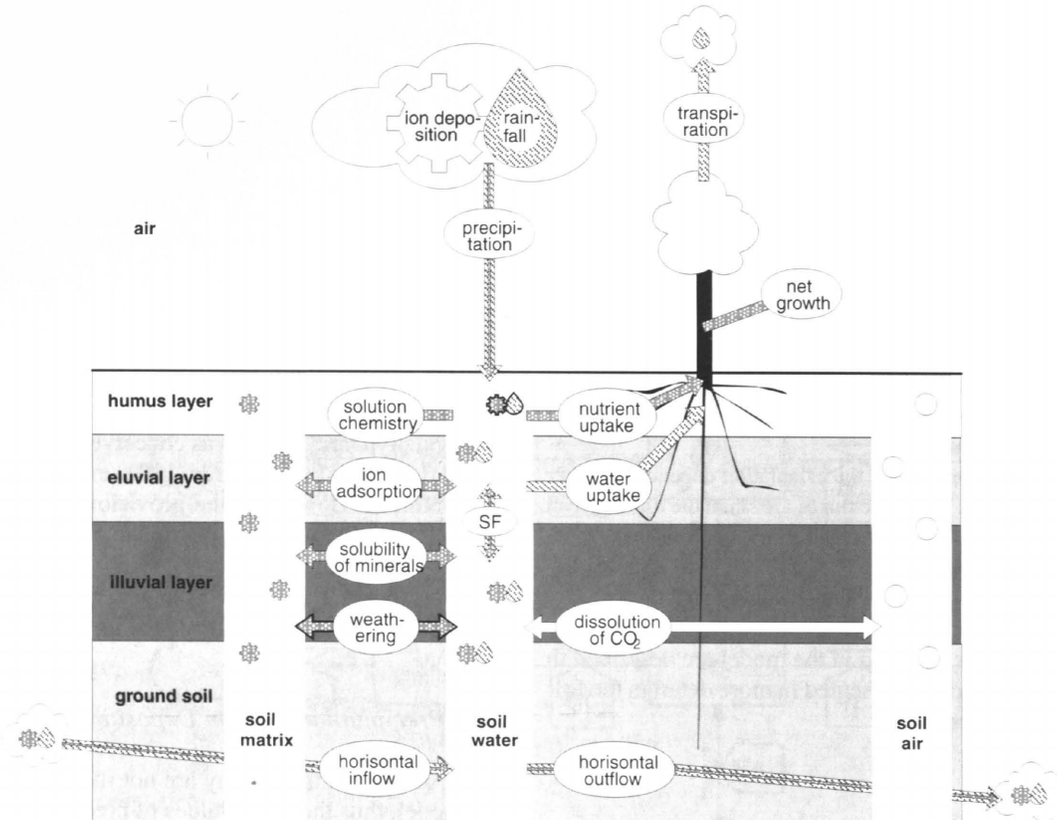

Fig. 1. Water and ion fluxes and the processes included to the model. Horisontal inflow and outflow include also the water flow in the soil surface. The abbreviation SF means water flow in the soil surface.

ration. At the same time the driving force of water uptake from each soil layer increases due to the decreasing plant water potential. The vertical distribution of the plant water uptake is determined by the vertical distributions in root amount and soil water potential.

6) For the organic acids a simple description has been given, since the model does not include decomposition of soil organic matter. Input of organic anions and accompanying protons is given in the throughfall data. The dissolved organic anions do not react with the soil matrix in the uppermost soil horizons. Below the top of the illuvial horizon they are retained in the soil matrix with aluminium.
7) The timestep of the calculation depends on water fluxes. When the fluxes are small the timestep can be e.g. one hour, but during large fluxes it can be e.g. one minute. The equilibrium of chemical reactions is solved numerically at each time step.

Processes included in the model are described in Fig. 1, and are presented in more detail in the following sections.

2.2 Hydrological Processes

Forces acting on water are often described by the *water potentials* Ψ_i [J kg^{-1}] or [J m^{-3}]. The soil water potential Ψ_t is commonly assumed to be the sum of the *matric potential* Ψ_m, *gravitational potential* Ψ_g, *osmotic potential* Ψ_o and *electrochemical potential* Ψ_e (Nielsen et al., 1986). Potentials may also be expressed on a unit weight basis, the term used then being *hydraulic head h* [m], which is $h = \Psi g^{-1}$ *(g = acceleration of gravity)*. In this work water potentials are expressed as hydraulic heads.

Assuming that water moves proportionally to the forces acting on it, we get the basic equation

$$q = -K\sum_i \frac{\partial h_i}{\partial x} A_e \qquad (1)$$

where q [l m^{-2} s^{-1}] is water flow, K [mm s^{-1}] is hydraulic conductivity, x [m] is distance and A_e [m^2 m^{-2}] is effective contact area.

The osmotic potential is spatially invariable in the soil, because there are no semipermeable membranes. The electrochemical potential is also assumed to be constant everywhere in soil, because soil solutions are relatively weak. Looking at the vertical water flow we now get an equation known as *Darcy's law* (1856)

$$q = -K\left(\frac{\Delta h_m}{\Delta z} + \frac{\Delta h_g}{\Delta z}\right) = -K\left(\frac{\Delta h_m}{\Delta z} - \frac{\Delta z}{\Delta z}\right) = -K\left(\frac{\Delta h_m}{\Delta z} - 1\right) \qquad (2)$$

where z [m] is vertical distance. In this statement the effective contact area is taken into account in the hydraulic conductivity term.

Originally Darcy's law was conceived for saturated flow only, but Richards (1931) extended it to unsaturated flow, with the provision that the hydraulic conductivity is a function of water content (or matric potential).

Water routes and all hydrological processes included in the model are presented in Fig. 2.

2.2.1 Precipitation and Ion Deposition

The processes in the canopy are not included to this model, thus the input values of precipitation and ion deposition are actually throughfall values.

The daily timing and the intensity of rain varies greatly, but the measurement usually includes only the daily precipitation value. In the model, the daily rainfall W_P [l m^{-2}] is divided into morning and afternoon fractions by the parameter R_{am} [%]. Morning rain starts at 24:00 and afternoon rain at 12:00. The assumed maximum rain intensity R_I [mm s^{-1}] determines the duration of the rainfall. The ion deposition is given as concentrations in precipitation.

The precipitation is added to the surface water storage W_{SW} [l m^{-2}]. Ion deposition is assumed to be dissolved in this water. The formation of snow cover and snow melting is not yet dynamically expressed, and the input of water and ions from snow to surface water and ion storages are given as input data.

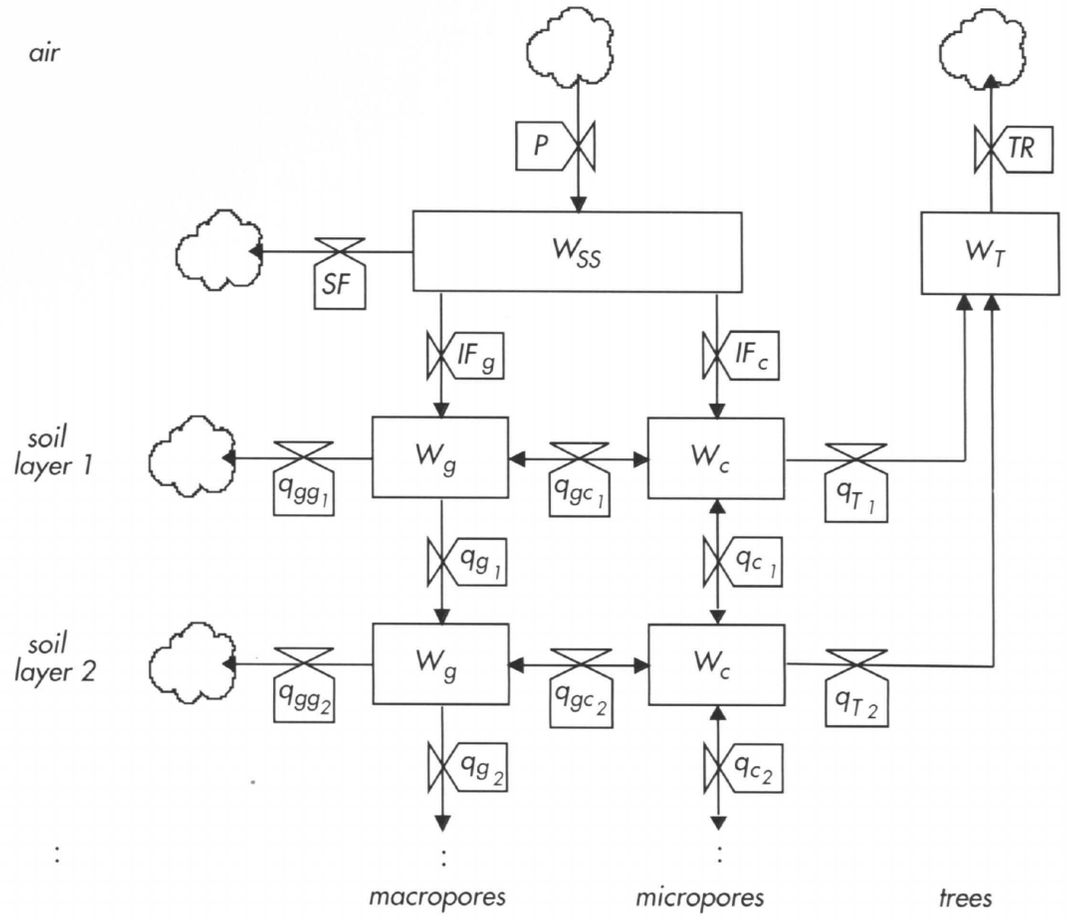

Fig. 2. A schematic presentation of soil water storages and flows between the storages. Indexes 1,2 etc. denote successive soil layers.
W_{SS} = surface water, W_g = water in macropores, W_c = water in micropores, W_T = water in trees, P = precipitation, SF = surface flow, IF_g = infiltration into macropores, IF_c = infiltration into micropores, TR = transpiration, q_g = percolation in macropores, q_c = percolation in micropores, q_{gc} = water flow between micro- to macropores.

2.2.2 Vertical Water Flow in Micropores

Matric and gravitation forces act on the vertical water flow in micropores q_c [l m^{-2} s^{-1}]. From Richards' equation we derive the formula for the water flow between subsequent soil layers (i and i+1)

$$q_{C_i} = -\overline{K}_{C_j}\left(\frac{h_{C_{i+1}} - h_{C_i}}{z_{i+1} - z_i} - 1\right) \qquad (3)$$

where $\overline{K}_c$ [mm s^{-1}] is the averaged hydraulic conductivity of micropores, h_c [m] is matric potential of micropore water and z [m] is distance of the soil layer midpoint from the soil surface.

The determination of the averaged hydraulic conductivity of micropores is based on an assumption that the matric water potential changes linearly between the midpoints of the subsequent layers. Taking into account the distance between the midpoints of the layers we get the water potential h_{cj} at the border j between the layers. The hydraulic conductivity is then calculated as the mean of the water flow resistances of the layers at the water potential h_{cj}

$$\overline{K}_{c_j} = \frac{2}{\frac{1}{K_{c_i}(h_{c_j})} + \frac{1}{K_{c_{i+1}}(h_{c_j})}} \quad (4)$$

where K_c [mm s^{-1}] is the hydraulic conductivity of micropores.

The matric potential of micropore water is a function of micropore water content. The relationship between water content and matrix potential is shown in the soil water retention curve (Fig. 3).

This study uses Van Genuchten's (1980) equation for the water retention curve

$$S_{ec} = \left[1 + (\alpha h_c)^n\right]^{-m} \quad (5)$$

where S_{ec} is effective saturation of micropores, and is specified as

$$S_{ec} = \frac{\theta_c - \theta_{rc}}{\theta_{sc} - \theta_{rc}} \quad (6)$$

where θ_c, θ_{sc} and θ_{rc} [l l^{-1}] are actual, saturated and residual water content of micropores. The curve is fitted to the observed values by parameters α, n and m.

Mualem (1976) has developed the predictive conductivity model, which introduces the relationship between matrix potential and hydraulic conductivity. Combining Mualem's and Van Genuchten's equations yields

$$K_c = K_{s_c} S_{ec}^{l} \left[1 - \left(1 - S_{ec}^{1/m}\right)^m\right]^2 \quad (7)$$

where K_{s_c} [mm s^{-1}] is saturated hydraulic conductivity of micropores. Mualem has estimated parameter l to be 0.5 for most soils.

2.2.3 Vertical Water Flow in Macropores

Gravitation is the driving force of vertical water flow in macropores. In this study all macropores are assumed to be equal in diameter, which is given by parameter d_g [m] for each soil layer, and furthermore macropores are assumed to be filled and emptied one by one. According to these assumptions the effective contact area between macropores of different layers is directly proportional to water saturation of macropores S_g of the upper layer. Now we get from the basic equation (1) a

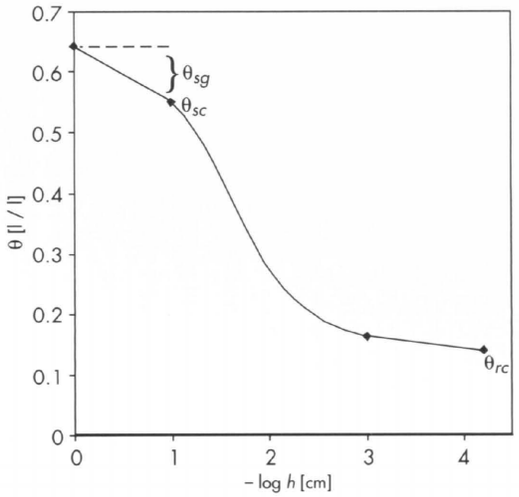

Fig. 3. An example of a soil water retention curve.
θ_{sg} = saturated water content of macropores
θ_{sc} = saturated water content of micropores
θ_{rc} = residual water content of micropores

formula for the vertical water flow in macropores q_g [l m^{-2} s^{-1}]

$$q_{g_i} = K_{s_{g_i}} S_{g_i} = K_{s_{g_i}} \frac{\theta_{g_i}}{\theta_{s_{g_i}}} \quad (8)$$

where K_{sg} [mm s^{-1}] is saturated hydraulic conductivity of macropores, and θ_g and θ_{sg} [l l^{-1}] are actual and saturated water content of macropores.

2.2.4 Water Flow between Macro- and Micropores

The water flow between macro- and micropores q_{gc} [l m^{-2} s^{-1}] is based on the matric and gravitation forces. The matric potential of macropore water is assumed to be zero. Usually water is flowing from macropores to micropores along matric potential gradient. However, close to saturation of micropores the gravitation is assumed to push water from micropores to macropores. This behaviour is described by a treshold matric potential parameter h_{gc} [m], so that under this treshold potential micropores suck water from macropores and above they loose water to macropores. The effective contact area between micro- and macro-

pores is the wall area of water saturated macropores. If water is flowing from micro- to macropores, then the total macropore wall area is accounted in the effective contact area. The water flow from macro to micropores derived from the basic equation (1), is then

$$q_{gc_i} = -K_{c_i} \frac{h_{c_i} - h_{gc_i}}{x_{gc_i}} A_{g_i} S_{g_i} \quad (9)$$

where x_{gc} [m] is average distance between macro- and micropores.

The area index of macropore wall A_g [m^2 m^{-2}] is calculated as follows

$$A_{g_i} = \frac{4\theta_{s_{g_i}} z_{S_i}}{d_g} \quad (10)$$

where z_S [m] is thickness of the soil layer.

2.2.5 Infiltration

The infiltration of the surface water into macropores of the first soil layer IF_g [l m^{-2} s^{-1}] is described correspondingly as vertical water flux in macropores (Equation 8), the only difference being that the effective contact area is unity

$$IF_g = K_{s_{g1}} \quad (11)$$

The infiltration of the surface water into micropores of the first soil layer has almost the same formula as vertical water flux in micropores (Equation 3), except that the hydraulic conductivity is determined by the first soil layer alone. The formula for the infiltration into micropores IF_c [l m^{-2} s^{-1}] is as follows

$$IF_c = -K_{c_1}\left(\frac{h_{c_1}}{z_{S_1}} - 1\right) \quad (12)$$

2.2.6 Horisontal Outflow

In a slope gravitation causes downhill flow, which we assume to take place in the macropores. This horisontal outflow q_{gg} [l m^{-1} s^{-1}] is

$$q_{gg_i} = \sin\beta\, q_{g_i} z_{S_i} = \sin\beta\, K_{sg_i} \frac{\theta_{g_i}}{\theta_{sg_i}} \cdot z_{S_i} \quad (13)$$

where β [°] is the average slope angle of the examined site.

The horisontal outflow takes place mainly in the deepest soil layers, thus it includes the description of groundwater flow. The parameter h_{gc} (in Equation 9) is crucial for the groundwater flow, because it affects the simulated production of macropore water from micropore water.

2.2.7 Surface Water Flow

The surface water storage is described as a pool. When the water amount exceeds the threshold volume of the pool, surface flow SF [l m^{-1} s^{-1}] begins. The equation is

$$SF = W_{SS} - z_{SS} \geq 0 \quad (14)$$

where W_{SS} [l m^{-2}] is water amount in soil surface and z_{SS} [mm] is the threshold height of the surface water pool.

2.2.8 Transpiration

Transpiration TR [l m^{-2} s^{-1}] is determined by the water vapour deficit in the air (Korpilahti 1988). The decrease in soil moisture content is assumed to decrease transpiration. This effect is described with the aid of the concept saturation of plant water storage (S_T). The transpired water is taken from plant water storage, which is receiving water from different soil layers, the divison between layers depending on soil water potential and the amount of roots in each layer (see Chapter 2.2.9). Transpiration is

$$TR = S_T K_L A_L \left[e_s(T) - e_s(T_{\min})\right] = \frac{\theta_T}{\theta_{s_T}} K_L A_L \left[e_s(T) - e_s(T_{\min})\right] \quad (15)$$

where K_L [mm s^{-1}] is stomatal conductance, A_L [m^2 m^{-2}] is leaf area index, e_s [g m^{-3}] is saturated water vapour at given temperature, T and $T_{\min}$ [°C] are actual and minimum air temperature of the day and θ_T and θ_{sT} [l l^{-1}] are actual and saturated water content of plant water storage.

The equation used for the calculation of the saturated water vapour is

$$e_s(T) = 5.0592 \cdot e^{0.06104 \cdot T} \quad (16)$$

The equation was derived by fitting a curve to the reported values (Handbook of chemistry ... 1948, p. 1912).

2.2.9 Plant Water Uptake

Plants are assumed to have a water storage, which affects transpiration and links it to the water uptake from the soil layers. Further, water potential of plant water storage h_T [m] is assumed to be a function of its saturation S_T

$$h_T = 10^2 + (1 - S_T)^5 \cdot 10^{4.2} \quad (17)$$

This formulation ensures that plants receive water also in dry periods, nevertheless the low soil moisture content may lead to undersaturation of the storage due to decreased conductivity. The behavior of the potential of plant water storage as a function of the saturation of the storage is presented in Fig. 4.

The water flow from soil to roots is described analogically to all the other flows in soil. The driving force of the water uptake is the difference between the potentials of the micropore water and plant water. The effective contact area depends on the root area. The equation of the water uptake q_T [l m^{-2} s^{-1}] is

$$q_{T_i} = -K_{c_i} \frac{h_T - h_{c_i}}{x_{cR_i}} A_{R_i} \geq 0 \quad (18)$$

where x_{cR} [m] is average distance between micropores and fine roots.

The root area index A_R [m^2 m^{-2}] is calculated as follows

$$A_{R_i} = \pi d_{R_i} z_{S_i} \rho_{R_i} L_{m_R} \quad (19)$$

where d_R [m] is average diameter of roots, r_R [kg m^{-3}] is root density and L_{mR} [m kg^{-1}] is ratio of root lenght to root mass.

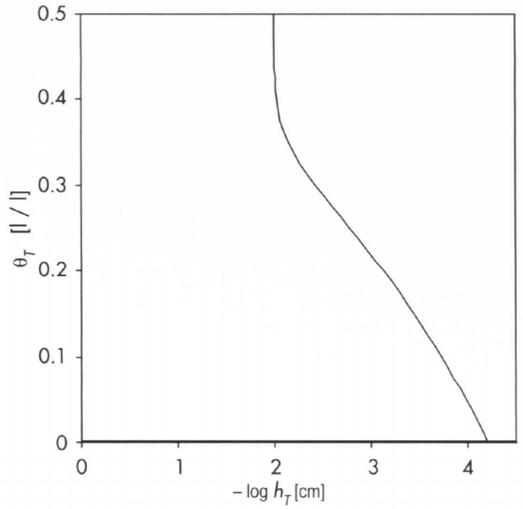

Fig. 4. The relation between the water content of trees, θ_T, and the water potential of trees, h_T.

2.3 Tree Growth

2.3.1 Growth

Tree stem growth TG [kg m^{-2} s^{-1}] is described as a function of air temperature and leaf area index

$$TG = v_{TG} A_L \sqrt{T_{mean} - T_{TG}}, T_{mean} - T_{TG} \geq 0 \quad (20)$$

where v_{TG} [kg °C$^{-1/2}$ m^{-2} s^{-1}] is growth rate, T_{mean} [°C] is mean air temperature of the day and T_{TG} [°C] is threshold growth temperature. The growth starts in spring when the threshold temperature sum TS_{spr} [°C] is achieved, and ends in autumn when the negative threshold temperature sum TS_{aut} [°C] is achieved.

2.3.2 Nutrient Uptake

All nutrients needed for the tree stem growth, are assumed to be taken up in a separate nutrient uptake process, which has no direct link with water uptake. In nutrient uptake the H$^+$-ion is extracted or taken up by the plant to maintain the charge balance in soil solution. The formula for the nutrient uptake NU [mol m^{-2} s^{-1}] of ion I from layer i is described as a function of both ion concentration and root area index

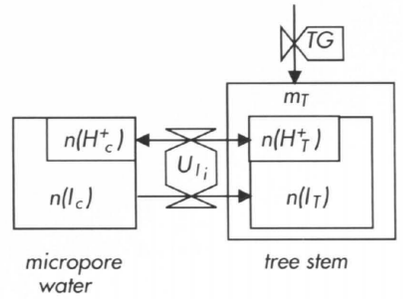

Fig. 5. A schematic presentation of the mass flows in tree growth (TG) and in nutrient uptake (U). m_T denotes tree stem biomass, $n(I_T)$ and $n(I_c)$ denote amount of cation I in tree stems and micropore solution respectively, and i denotes soil layer.

$$NU_{I_i} = v_{NU_I} [I_c]_i A_{R_i} \quad (21)$$

where $[I_c]$ [mol l^{-1}] is concentration of ion I in micropore water (Fig. 5).

The uptake rate v_{NUI} [l m^{-2} s^{-1}] of ion I is determined so that the nutrient need for growth is always satisfied

$$v_{NU_I} = \frac{[I_T] TG}{\sum_1^{n_S} ([I_c]_i A_{R_i})} \quad (22)$$

where $[I_T]$ [mol kg^{-1}] is content of ion I in tree stems and n_S is number of soil layers accounted in the simulation.

2.4 Soil Chemical Processes

The dynamics of chemical reactions are usually described by thermodynamic equilibrium equations with two kinds of parameters: equilibrium coefficients k and rate coefficients v. As an example the thermodynamic equilibrium equation of chemical reaction

$$aA + bB \rightleftarrows xX + yY \quad (23)$$

is

$$k = \frac{\{X\}^x \{Y\}^y}{\{A\}^a \{B\}^b} \quad (24)$$

Bracets { } denote activities. The equation of ion mass flow C derived from equilibrium equation (24) is

$$C = v \left(k \{A\}^a \{B\}^b - \{X\}^x \{Y\}^y \right) \quad (25)$$

The calculation algoritms of the soil chemical processes are formulated so that the modeled reactions reach their equilibriums in preset accuracy (simulated equilibrium coefficient is within e.g. ±5 % of the given value) at every calculation time step. Thus the following mass flow equations are introduced without rate coefficients. Weathering is an exception, so that it is described as a steady state process driven by a rate coefficient.

All the solution chemistry processes are assumed to take place in the micropores. A constant soil temperature (10 °C) is assumed for the chemical reactions, because heat transfer in the soil is not included. Ion activity coefficients are estimated by the extended *Debye-Hückel* equation (Lindsay 1979).

2.4.1 Water Autoprotolysis

The water autoprotolysis

$$H_2O \Leftrightarrow H^+ + OH^- \quad (26)$$

is formulated as a mass flow C_{H_2O} [mol l^{-1} s^{-1}], the equation being

$$C_{H_2O_i} = k_{H_2O} - \{H^+_c\}_i \{OH^-_c\}_i \quad (27)$$

where k_{H_2O} is equilibrium constant of the reaction, usually called the ion product of water.

2.4.2 Carbon Dioxide Dissolution and Carbonic Acid Dissociation

Carbon dioxide gas is an important element in soil, affecting solution acidity and indicating the vitality of the soil organisms. Changes in the partial pressure of carbon dioxide p_{CO_2} [%] in soil depend greatly on the activity of microbes decomposing organic soil matter. As the decomposition is not described as a dynamic process, the changes of CO_2 partial pressure cannot be de-

scribed dynamically either. Thus the partial pressure of CO_2 depends on the simulated season, the idea being based on the soil air studies of Magnusson (1992).

CO_2 partial pressure is assumed to follow the sinus curve, the parameters being the lengths of the periods t [days] and partial pressures in the periods p_{CO_2} [%] (Fig. 6).

Carbon dioxide dissolves in water, forming both dissolved carbon dioxide ($CO_2°$) and undissociated carbonic acid ($H_2CO_3°$). However, it is common to describe only one dissolution reaction, in which all the dissolved carbon dioxide forms carbonic acid

$$CO_2(g) + H_2O \Leftrightarrow H_2CO_3^\circ \quad (28)$$

Carbonic acid dissociates further to a bicarbonate ion

$$H_2CO_3^\circ \Leftrightarrow H^+ + HCO_3^- \quad (29)$$

The mass flow equations for reactions (28) and (29) are

$$C_{CO_i} = k_{CO}(T)p_{CO_{2i}} - \left[\left(H_2CO_3^\circ\right)_c\right]_i \quad (30)$$

$$C_{CA_i} = k_{CA}\left[\left(H_2CO_3^\circ\right)_c\right]_i - \left(H^+{}_c\right)_i\left\{\left(HCO_3^-\right)_c\right\}_i \quad (31)$$

2.4.3 *Hydrolysis of Aluminium Compounds and Aluminum Complexation with Sulfate*

In aqueous solutions aluminium (Al^{3+}) is surrounded by water molecules ($Al(H_2O)_6^{3+}$). This hexahydronium ion buffers the pH of the solution by releasing protons from the coordinated water molecules. The common hydrolysis reactions of aluminium in podzolic soil solutions are

$$Al^{3+} + H_2O \Leftrightarrow AlOH^{2+} + H^+ \quad (32)$$

$$Al^{3+} + 2H_2O \Leftrightarrow Al(OH)_2^+ + 2H^+ \quad (33)$$

$$Al^{3+} + 3H_2O \Leftrightarrow Al(OH)_3 + 3H^+ \quad (34)$$

Aluminium forms also other complexes with fluoride, sulfate and nitrate. Fluoride and nitrate

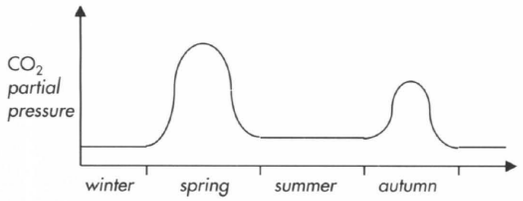

Fig. 6. Annual changes in the partial pressure of carbon dioxide in the soil air. The height and the length of the spring and autumn peaks as well as the base concentration can be determined by the model user.

are often not significant as complexing agents due to their low concentrations in podzolic soils, and only sulfate needs to be considered. The aluminium complexation with sulfate is

$$Al^{3+} + SO_4^{2-} \Leftrightarrow AlSO_4^+ \quad (35)$$

The mass flow equations for hydrolysis and complexation of aluminium are

$$C_{AlOH_i} = k_{AlOH}\left\{Al^{3+}{}_c\right\}_i - \left\{AlOH^{2+}{}_c\right\}_i\left\{H^+{}_c\right\}_i \quad (36)$$

$$C_{Al(OH)_2 i} = k_{Al(OH)_2}\left\{Al^{3+}{}_c\right\}_i - \left\{\left(Al(OH)_2^+\right)_c\right\}_i\left\{H^+{}_c\right\}_i^2 \quad (37)$$

$$C_{Al(OH)_3 i} = k_{Al(OH)_3}\left\{Al^{3+}{}_c\right\}_i - \left[\left(Al(OH)_3\right)_c\right]_i\left\{H^+{}_c\right\}_i^3 \quad (38)$$

$$C_{AlS_i} = k_{AlS}\left\{Al^{3+}{}_c\right\}_i\left\{\left(SO_4^{2-}\right)_c\right\}_i - \left\{\left(AlSO_4^+\right)_c\right\}_i \quad (39)$$

2.4.4 *Mineral Solubility*

The dissolution of gibbsite, alunite, kaolinite and gypsum are included in the model

$$Al(OH)_3(c) + 3H^+ \Leftrightarrow Al^{3+} + 3H_2O \quad (40)$$

$$KAl_3(OH)_6(SO)_{42} + 6H^+ \Leftrightarrow 3Al^{3+} + K^+ + 2SO_4^{2-} + 6H_2O \quad (41)$$

$$Al_2Si_2O_5(OH)_4 + 6H^+ \Leftrightarrow 2Al^{3+} + 2H_4SiO_4 + H_2O \quad (42)$$

$$CaSO_4 \cdot 2H_2O \Leftrightarrow Ca^{2+} + SO_4^{2-} + 2H_2O \quad (43)$$

The mass flow equations for the solubility reactions are

$$C_{gibb_i} = k_{gibb}\left\{H^+{}_c\right\}_i^3 - \left\{Al^{3+}{}_c\right\}_i \quad (44)$$

$$C_{alun_i} = k_{alun}\left\{H^+{}_c\right\}_i^6 - \left\{Al^{3+}{}_c\right\}_i^3\left\{K^+{}_c\right\}_i\left\{\left(SO_4^{2-}\right)_c\right\}_i^2 \quad (45)$$

$$C_{kaol_i} = k_{kaol}\left\{H^+{}_c\right\}_i^6 - \left\{Al^{3+}{}_c\right\}_i^2\left[\left(H_2SiO_4\right)_c\right]_i^2 \quad (46)$$

$$C_{gyps_i} = k_{gyps} - \left\{Ca^{2+}{}_c\right\}_i\left\{\left(SO_4^{2-}\right)_c\right\}_i \quad (47)$$

2.4.5 *Cation Exchange*

The exchangeable cations considered in this study are H^+, Al^{3+}, Ca^{2+}, Mg^{2+}, K^+, Na^+, NH_4^+. The change in the cation exchange capacity due to the difference between the total and the exchangeable acidity is not accounted for at this stage of the model.

The cation exchange reaction between ions I and J is

$$Z_J I + Z_I J_a \Leftrightarrow Z_J I_a + Z_I J \quad (48)$$

where Z_I [$mol_c\ mol^{-1}$] is charge of ion I and I_a [mol kg^{-1}] is the quantity of ion I adsorbed. The main uncertainty in describing the reaction equilibrium is the definition of adsorbed ion activity. Here the assumption of Gaines and Thomas (1953) is followed, and the activity of adsorbed cation I is related to its equivalent fraction E_I

$$E_I = \frac{I_a}{\sum_I I_a} \quad (49)$$

where I = [H, Al, Ca, Mg, K, Na, NH_4]. Thus the mass flow equation of cation exchange becomes

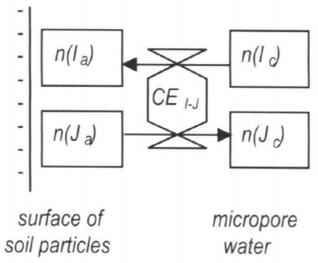

Fig. 7. A schematic presentation of the mass flows in cation exchange (*CE*) reactions, I and J denote different cations.

$$CE_{I-Ji} = k_{I-Ji}\left\{I_c\right\}_i^{Z_J} E_{J_i}{}^{Z_I} - E_{I_i}{}^{Z_J}\left\{J_c\right\}_i^{Z_I} \quad (50)$$

where k_{I-J} is equilibrium coefficient (or selectivity coefficient) of cation exchange between ions I and J (Fig. 7).

2.4.6 *Sulfate Adsorption*

In forest soil solutions phosphate (PO_4^{3-}), sulfate (SO_4^{2-}) and nitrate (NO_3^-) are biologically the most important anions. The phosphate ion has not been included in this model yet, because of the many specific features of the phosphate reactions. Because nitrate is mainly immobilized biologically and the adsorption power of the nitrate ion is the weakest of the three, only the adsorption reaction of the sulfate ion is included in the model.

A common way to present stoichiometric equation of sulfate adsorption is

$$SO_4^{2-} + 2OH_a \Leftrightarrow \left(SO_4\right)_a + 2OH^- \quad (51)$$

Equilibrium between dissolved and adsorbed sulfate is described by the Langmuir isotherm. The mass flow equation for sulfate adsorption SA [mol $kg^{-1}\ s^{-1}$] is then

$$SA_i = \frac{\left[\left(SO_4\right)_{a-\max}\right]_i\left[\left(SO_4^{2-}\right)_c\right]_i}{k_{SA_i} + \left[\left(SO_4^{2-}\right)_c\right]_i} - \left[\left(SO_4\right)_a\right]_i \quad (52)$$

where $[(SO_4)_{a-max}]$ [mol kg^{-1}] is maximum sulfate adsorption capacity of the soil and k_{SA} [mol l^{-1}] is equilibrium coefficient of the sulfate adsorption.

2.4.7 Formation and Precipitation of Organic Complexes

A simple description of organic acid reactions is given, since decomposition is not included in this model yet. The input of organic anions and accompanying protons is given in the throughfall data. The equation of organic complex formation is

$$3R^- + Al^{3+} \Leftrightarrow R_3Al \tag{53}$$

and the mass flow equation for the reaction is

$$OC_i = \begin{cases} 3\left[R^-{}_c\right]_i, 3\left[R^-{}_c\right]_i \le \left[Al^{3+}{}_c\right]_i \\ \left[Al^{3+}{}_c\right]_i, 3\left[R^-{}_c\right]_i > \left[Al^{3+}{}_c\right]_i \end{cases} \tag{54}$$

The first layer where organic complexes are formed and retained from the solution to the soil matrix is given by parameter n_{OC}. This complexation and retention may also take place in the micropores of the lower layers if organic anions are transferred there by macropore flow.

2.4.8 Weathering

Minerals are described as breaking down completely; thus the release of ions depends on their concentrations in the minerals. Mineral weathering MW [kg m^{-2} s^{-1}] of ion I is described as a steady-state process

$$MW_{Ii} = v_{MW_i}\left[I_M\right] \tag{55}$$

where v_{MW} [kg m^{-2} s^{-1}] is weathering rate and $[I_M]$ [mol kg^{-1}] is concentration of ion I in the minerals.

3 Application of the Model to Rudbäcken

3.1 General

A dynamic process-oriented model, based on general theories, can be used to analyze the outcome of various assumptions of the system inputs and structure. In acidification analysis the changing inputs may be the amounts of various ions in deposition, whereas in an analysis of climate change effects the precipitation and temperature should be considered. The theory or empirical evidence regarding the system structure and function are sometimes so poorly understood that a precise expression for the processes involved is not obvious. Here, the water flow in soil and the effect of flow in macropores on soil solution ion concentrations are processes for which no empirical evidence is available. The general equilibrium assumptions concerning cation exchange and aluminium dissolution were assumed here to be valid in micropores, while no chemical reactions were assumed in macropores. The effects of various water flow systems to solution ion concentrations were then considered. The observed cation concentrations in the horizons of a podzolic soil were used as a background and as comparative data, the solutions being collected with suction lysimeters during the growing season of 1991.

The concept macropore flow is used here to study the flow of solution not chemically equilibrated with the soil matrix. The macropore flow can be defined here as a flow mainly affected by the gravitational potential and less by the matrix potential. However, capillary forces have a small impact on the flow through the conductivity term K_g. The macropore flow in the case in which there is no flow in micropores may be compared to a flow of water which exceeds the water content in field capacity, as in the leaching models of Terkeltoub and Babcock (1971) and Burns (1974). The descriptions of piston flow in the mobile water phase followed by equalization of the concentrations in mobile and immobile phases (Addiscott 1977) or solute diffusion between the phases (Addiscott 1982) are also comparable to the combination of macropore and micropore flows described in this study. Addiscott and Wagenet (1985) have introduced and discussed various solute leaching models.

3.2 Simulated Cases

Various proportions of macropore flow were assumed in the simulated cases A, B and C. Case A with no macropore flow was selected as the reference case, because macropore flow is often neglected in models of forest soils, and because the assumption of chemical equilibrium between the soil and the soil solution is usually used in the soil acidification models. In case B high conductivity in macropores was assumed (see Chapter 3.4), resulting in a high proportion of water inflow to the E and Bs1 horizons as macropore flow, not equilibrated with the chemical system of the horizons above. In case C the flow in micropores was assumed to be neglible compared to flow in macropores. The only exit for water from the micropores of each horizon was to plant roots, and so no leaching of the exchangeable cations occurred in this case.

The simulated period started in April and ended in December. Early spring was selected for the start, so that the snow cover was assumed to melt a week later, the thaw lasting two weeks. After this, the precipitation was assumed to be liquid water until the end of the simulation. We simulated eight soil layers, corresponding to O, E, Bs1 and Bs2 horizons, and the ground soil divided to four layers. The thicknesses of the layers were 5 cm, 5 cm, 10 cm, 20 cm, 30 cm, 30 cm, 50 cm and 50 cm respectively.

3.3 Site Description, Experimental Design and Chemical Analyses

For the purpose of model comparisons with environmental data an intensive data collection for soil and soil solution data was carried out in a forested catchment. Daily precipitation and weekly throughfall of water and ions were measured by the National Board of Waters and Environment (Kämäri et al. 1992).

The catchment of lake Rudbäcken is situated in Siuntio in southern Finland (60°08'N, 24°18'E). The mean temperature and precipitation 1961–1990 were 4.6 °C and 651 mm respectively, at the Helsinki-Vantaa airport 40 km west of the site. Site S2, which is analysed in this study, is situated in the catchment in the middle of a slope (angle 15°, length 80 m). The stand consists of 68 % *Picea abies*, 22 % *Pinus sylvestris* and 10 % *Betula pendula*, *Alnus glutinosa* and *Populus tremula*. The average height of the trees is 27 m and the average age of the spruce is about 85 years, stand volume being about 300 m^3 ha^{-1}. The ground vegetation consists of *Vaccinium myrtillus* (cover 32 %), *Maianthemum bifolium* (6 %), *Melampyrum sylvaticum* (2 %) and *Melampyrum pratense* (2 %). The most abundant mosses are *Pleurozium schreberi* (30 %) and *Dicranum scoparium* (22 %). The soil profile has been developed on a glacial till. However, the top horizons have been partly outwashed of fine material, because the sea shore was at this level between 8800 and 8000 B.C. In the illuvial horizon the soil consists of 11 % gravel, 70 % sand, 15 % of silt and 4 % clay. The corresponding figures for the ground soil are 10 %, 43 %, 33 % and 14 %.

The composite sample of the throughfall was collected from 18 funnels installed in the slope in three rows (Kämäri et al. 1992). The soil water potential in the slope was measured with 35 sets of four tensiometers (depths 5, 25, 50 and 75 cm, Jauhiainen and Nissinen 1994). The observations of the two sets nearest to the lysimeters were used in this analysis. The water retention curves of each soil horizon were measured from the soil samples taken from the same wall of a pit in which the lysimeters were installed (Jauhiainen and Nissinen 1994). The conductivity was measured in the field with the SMS Tension Infiltrometer (Mecke 1994).

Suction lysimeters (PTFE, Prenart Equipment ApS) were used to obtain soil solution samples. They were installed at depths of 5 cm (E-horizon), 15 cm (Bs1), and 25 cm (Bs2) in the wall of a pit. The solution sample was collected at irregular intervals in glass bottles (first 2 L Pyrex-bottles and after July in 300 ml Pyrex-erlenmeyers) and during the dry seasons in centrifuge tubes (polystyrene, 10 mL). The maximum vacuum was –750 mbar. pH was measured immediately in the laboratory from a sub-sample before and after bubbling with ambient air. The concentration of reactive Al was measured within 48 hours with pyrocatechol violet (Bartlett et al. 1987). The rest of the solution was stored in a freezer until Ca and Mg analyses with an atomic absorption spectrophotometer and K with a flame spectrophotometer. The anions SO_4^{2-}, NO^{3-} and Cl^- were measured with HPLC for some sampling occasions (Nissinen et al. 1998).

The Al concentration was divided by an iteration procedure into Al^{3+}, $Al(OH)^{2+}$, $Al(OH)_2^+$ and $Al(OH)_3^0$. Fractioning was done using the solution H^+ activity, estimated ionic strength and activity coefficients of Al ions, and hydrolysis equilibrium coefficients k_{AlOH1}, k_{AlOH2}, and k_{AlOH3} (see Equations 32–39 in Chapter 2.4.3.).

A soil sample for chemical measurements was taken from each hole, which was made for a lysimeter. The soil was air-dried and used for determining the exchangeable cations with 0.1 M $BaCl_2$ (Nissinen et al. 1998, Table 1).

3.4 Model Input and Parameter Values

The precipitation was 800 mm in 1991, and 495 mm during the simulated period. The daily water input to the soil (or throughfall) was calculated by multiplying the daily precipitation value by a factor of 0.75 (Hyvärinen 1990). The measured ratio at the site was low, 0.62, because the bottles were too small to collect all water during heavy rains. The weekly throughfall of each ion or element was divided into daily values with the help of daily precipitation (Kämäri et al. 1992). The anion deficit was assumed to be organic anion.

The initial values (on April 1) of the simulated cation concentrations in the soil solution were

Table 1. Initial values of adsorbed ions.

	H^+	Al^{3+}	Ca^{2+}	Mg^{2+} [$mmol_c$ kg^{-1}]	K^+	Na^+	NH_4^+	SO_4^{2-}
O	31.4	26.6	131.6	17.1	10.2	5.1	4.5	0
E	1.713	30.365	3.288	0.796	0.943	0.943	1	0.5
Bs1	0.605	11.78	1.437	0.33	0.215	0.215	0.2	2
Bs2	0.388	6.199	1.946	0.308	0.574	0.574	0.1	2
C1	0.537	8.706	8.93	2.734	0.819	0.819	0.1	4

Table 2. Parameters of soil water retention curve and water flow in soil.

	θ_s [l l^{-1}]	θ_r [l l^{-1}]	θ'_s [l l^{-1}]	θ'_r [l l^{-1}]	a	n	m	K_{sg} [cm h^{-1}]	K_{sc} [cm h^{-1}]
O	0.637	0.172	0.317	0.173	0.046	1.953	0.397	120	60
E	0.642	0.141	0.594	0.148	0.037	1.598	0.576	60	0.4
Bs1	0.507	0.072	0.507	0.122	0.017	1.379	0.891	60	0.4
Bs2	0.54	0.088	0.54	0.144	0.033	1.208	0.585	60	0.4
C1	0.428	0.325	0.422	0.325	0.014	0.783	0.930	30	0.01

calibrated so that all chemical reactions were close to their equilibria, and the simulated total charge was close to observed on May 15. The initial sulfate concentration was also calibrated to fit the concentration observed in each horizon on May 15. Nitrate and chloride were given the same concentrations as in the throughfall.

The parameters of the water retention curve, the hydraulic conductivities (Table 2), and the parameters of transpiration were derived mainly from measurements. The pore space of macropores was estimated from the water retention curve as the difference between pF-values 0 and 1 (Fig. 3). The saturated conductivity in micropores K_{sc} was the same in cases A and B, and was set to zero in case C. The saturated conductivity in macropores K_{sg} was estimated from the conductivity in coarse sand. In case A this term was set zero for mineral soil layers. The root distribution was based on Jauhiainen and Nissinen (1994) and Majdi and Persson (1993). The transpiration is regulated mainly by the leaf area index A_L and the stomatal conductance K_L. The A_L was estimated to be 5, and the value for stomatal conductance was set to 1.3 mm s^{-1} (Berninger and Hari 1993).

The distance-parameter x_{gc} in the flow between micro- and macropores was calibrated so that the simulated water content followed closely the observed low water contents in case B. The values were 500 m in the humus layer and 10 m in the mineral soil layers. The distance parameter x_{cR} was 100 m in case A and 1000 m in case B. These were calibrated together with the exponents in Equation 17. In calibration, we assumed that water potential in plant decreases only slowly with decreasing plant water saturation when the saturation is high, but starts to decrease exponentially when the saturation decreases to a low level. The observed water potentials during the driest periods, in mid July and early August, were used for the calibration of the parameters.

The simulated transpiration was 319 mm. Together with the assumed interception, 25 % of precipitation, this results in evapotranspiration of 443 mm in 1991, which is 89 % of the precipitation of 495 mm. Assuming the same fraction of precipitation to be lost by evaporation of the intercepted water in the winter, the annual evapotranspiration would cover 65 % of the annual precipitation. This ratio is somewhat higher than the mean value, about 60 %, for the whole of southern Finland. However, this areal average value includes also non-forested areas (Vakkilainen 1968).

Table 3. Gaines-Thomas coefficients for cation exchange and coefficients for sulfate adsorption.

	k_{H-Al} $\cdot 10^6$	k_{Al-Ca}	k_{Ca-Mg}	k_{Mg-K} $\cdot 10^{-3}$	k_{K-Na}	k_{Na-NH4}	$(SO_4)_a^{max}$ [$mmol_c\ kg^{-1}$]	k_{SA} [$mmol_c\ l^{-1}$]
O	1.23	$6.18 \cdot 10^{-3}$	6.31	1.34	1	1	0	0
E	24.1	6.44	3.87	0.152	1	1	1	0.12
Bs1	49.2	14.6	5.25	0.291	1	1	4	0.12
Bs2	2.93	0.569	8.62	0.221	1	1	4	0.13
C1	2.11	1.62	1.87	0.188	1	1	8	0.13

Table 4. Equilibrium coefficients of solution chemistry.

Reaction	Equilibrium coefficient symbol	log k
$H_2O \Leftrightarrow H^+ + OH^-$	k_{H2O}	–14.53
$CO_2(g) + H_2O \Leftrightarrow H_2CO_3^0$	k_{CO}	–1.27
$H_2CO_3^0 \Leftrightarrow H^+ + HCO_3^-$	k_{CA}	–6.464
$Al^{3+} + H_2O \Leftrightarrow AlOH^{2+} + H^+$	k_{AlOH}	–5.285
$Al^{3+} + 2H_2O \Leftrightarrow Al(OH)_2^+ + 2H^+$	$k_{Al(OH)2}$	–9.791
$Al^{3+} + 3H_2O \Leftrightarrow Al(OH)_3 + 3H^+$	$k_{Al(OH)3}$	–15.787
$Al^{3+} + SO_4^{2-} \Leftrightarrow AlSO_4^+$	k_{AlS}	3.2
$Al(OH)_3(c) + 3H^+ \Leftrightarrow Al^{3+} + 3H_2O$	k_{gibb}	10.175

Annual variation of pCO_2 was estimated as sine waves having maxima in the spring and in the autumn. According to Magnusson's (1992) data the peak concentrations on freely drained forest soils were around 1 % (volumetric %), occurring after the thaw in April and May and in the late summer in August and September. Between the peaks the concentration was around 0.1–0.5 %. In simulations a base-concentration of 0.1 % and a peak-concentration of 1 % were used.

The parameters of the growth function were calibrated so that the annual stem growth was 5 $m^3 ha^{-1} a^{-1}$. The uptake of nitrate is described assuming that trees take all the nitrate from the soil solution in the uppermost horizons. According to our observations, the nitrate concentration in the soil solution is near zero. In the brooks of the Rudbäcken catchment the nitrate concentrations have been below 10 µmol/l in 1991–1994, except four observations yielding concentrations of 10–50 µmol/l (Kämäri et al. 1992). Compared to sulfate concentrations, 200–600 µmol/l, the nitrate concentrations are thus very small.

No estimates of weathering have been done at the site, so we selected a low weathering value (16 $mmol_c\ m^{-2}\ a^{-1}$), based on a study of seven sites in Scandinavia (Sverdrup and Warfvinge 1993). The proportions of each base cation were based on the same study: Ca^{2+} 42 %, Mg^{2+} 23 %, K^+ 11 % and Na^+ 24 %. The weathering rate is assumed to be highest in the topsoil, the rates being 25 % slower in layer Bs2 and 50 % slower in layers C1 and C2.

Gaines-Thomas cation-exchange coefficients were determined using the measured contents of exchangeable cations in the soil horizons and the measured cation concentrations in the soil solution samples. The horizon-specific median value of each coefficient was used in the simulations (Table 3). However, the exchange coefficients were not calculated separately for each Al hydroxide species, as these were not measured directly. Instead, all Al was assumed to react as if it was Al^{3+}. The same assumption was made in the simulations with the model. The parameters of sulfate adsorption were calibrated so that they produced the level of the observed concentrations in each horizon. The parameters of aluminium dissolution and hydroxide formation in the soil solution were taken from the literature (Lindsay 1979, Table 4).

4 Results and Discussion

4.1 Soil Water Content

The simulated time and depth patterns of the soil water content in the reference case A (Fig. 8) are considered first, followed by a comparison with the observations and other cases.

Soil water content is high in the spring, and water flows rapidly through each horizon. Transpiration starts to diminish the soil water storage in the early summer, and during the summer months the soil is relatively dry. The upper soil horizons have lower water content and lower water potential than

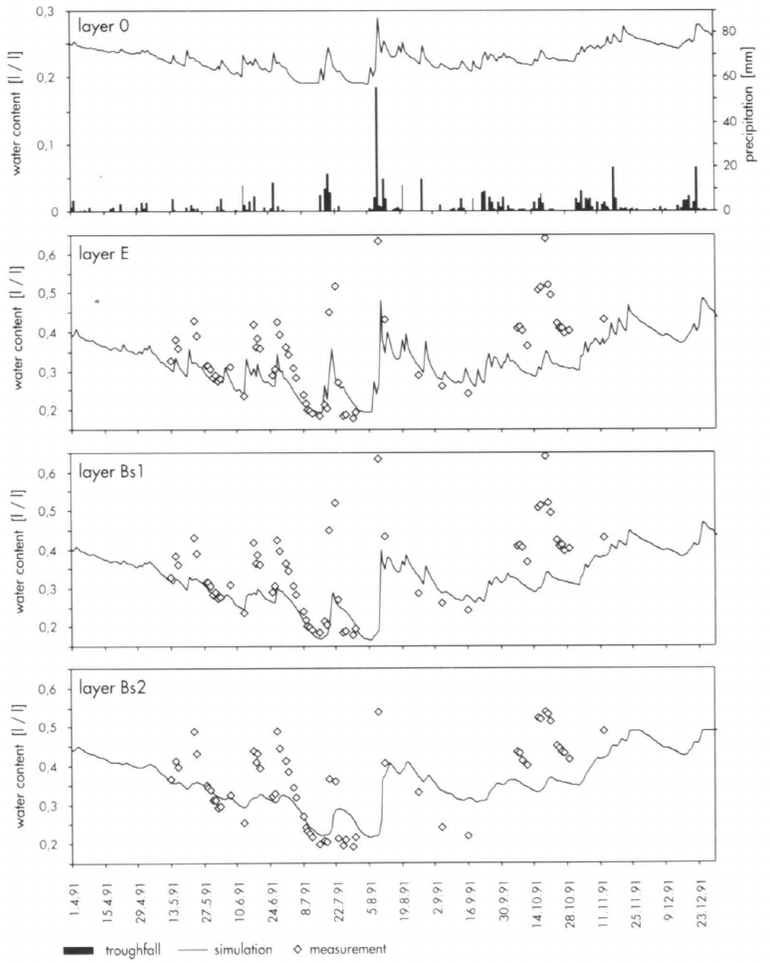

Fig. 8. Simulated (line) and observed (dots) water contents in case A. In layer 0 the bars represent the amount of throughfall.

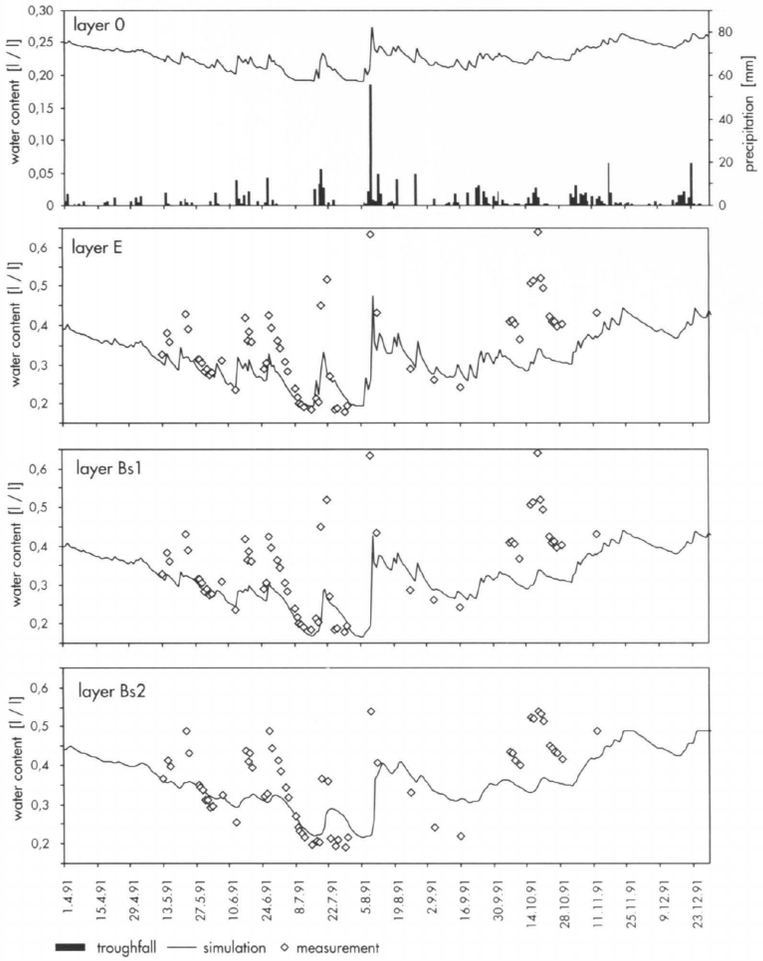

Fig. 9. Water content in case B, otherwise as in Fig. 8.

the layers deeper in soil, excluding some heavy rain events. The water content is also more variable in the topsoil compared to the deeper soil layers. The amount of soil water, as well as the vertical water flow, increases again in September. At the end of the simulation period the water content in each horizon is close to the initial value.

When comparing the simulated soil water contents with the measured values, at the first glance there seems to be a serious mismatch. After each rain episode the change in the measured soil water content is much more pronounced compared to the simulated one. When analysing different explanations for this mismatch, we calculated also the expected change in the soil water content, if the amount of water in one rain episode would be evenly distributed in a 50 cm thick soil layer. This calculation showed, that after each major rain event, the measured change in soil water content was much higher than expected. Based on this, and some evidence in litterature, we concluded that the tensiometers do not give reliable values of soil water content shortly after the rain episodes. When the timing of the peaks (instead of the actual hights) is considered we can find a reasonably good fit between measured and simulated values after each rain event. And further, if the periods between rain events are considered we can see that the simulated water content follows closely the observed water contents over the whole

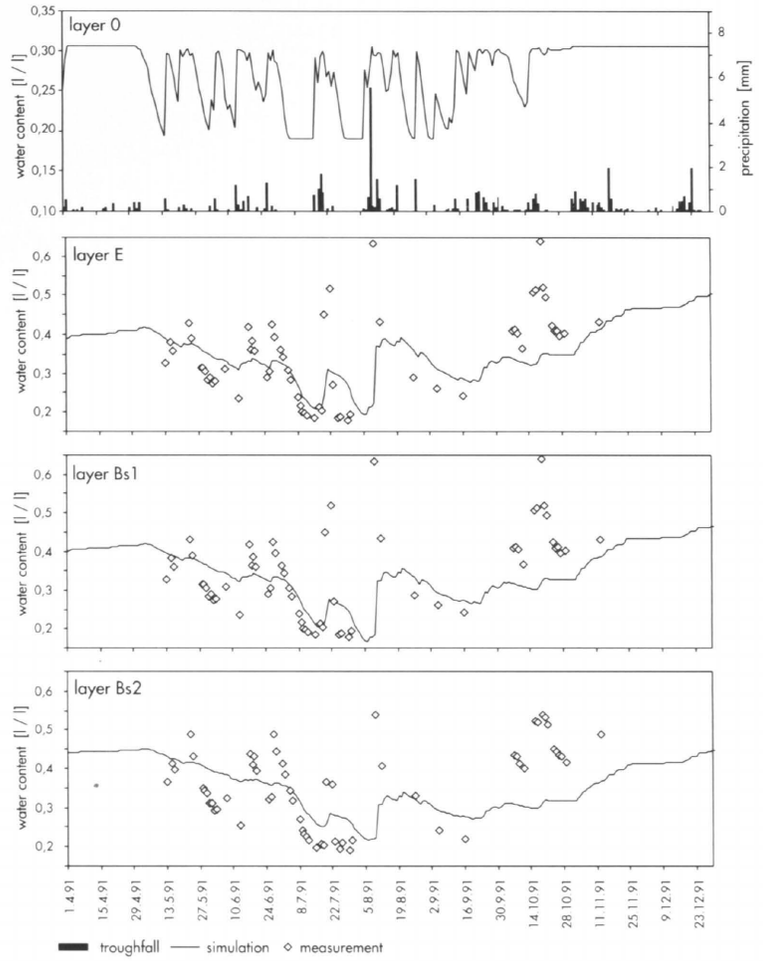

Fig. 10. Water content in case C, otherwise as in Fig. 8.

period between May and September (Fig. 8).

The simulated temporal and depth patterns of water contents in cases A and B are almost identical (Figs. 8 and 9). In case C the uppermost soil layer behaves in a different manner compared to the other cases. In the mineral soil layers the soil water content is higher in the early summer, reaching the same level as in the other cases at the beginning of August (Fig. 10). After this the soil water content behaves quite similarly in all cases.

Based on the measurements, it is not possible to decide, which of the cases corresponds best with the actual water content of the soil. In general the behavior of soil water content is very similar in all studied cases, since whatever flow route was selected after rainfall, the field capacity of different soil horizons was reached rapidly, and after this the main cause for changes in soil water content was transpiration, which was similar in all cases. However, the water content of cases A and B follows more closely low water contents than case C, in which the simulated soil water content is higher than the observed during the spring and summer.

4.2 Water Flow Routes

Opposite to the quite similar estimations of soil water content, the estimated amount of water flow-

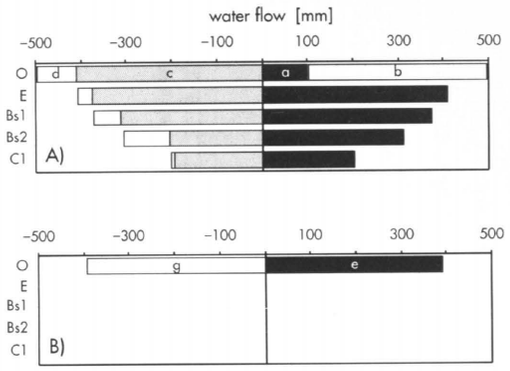

Fig. 11. Simulated water budgets in case A, expressed as water amounts flown into micro- and macropores (positive flows) and out from micro- and macropores (negative flows),
A) micropores: a) flow from layer above into micropores; b) flow from macropores into micropores; c) flow in micropores into layer below; d) water uptake
B) macropores: e) flow in macropores from layer above; f) flow in macropores to layer below; g) flow from macropores to micropores

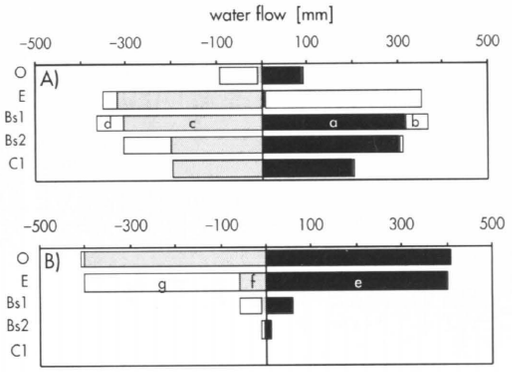

Fig. 12. Simulated water budgets in case B, otherwise as in Fig. 11.

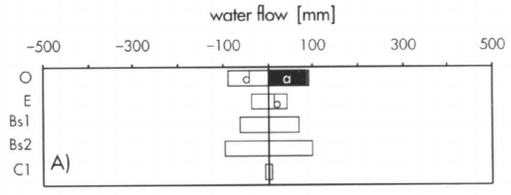

Fig. 13. Simulated water budgets in case C, otherwise as in Fig. 11.

ing through each soil layer within micropores is very different in cases A, B and C. In case A all of the water in throughfall (485 l m^{-2}) is transferred into the micropores in the uppermost soil horizon, and movement of water occurs only in the micropores (Fig. 11). About 400 l m^{-2} water reaches the layer E and 370 l m^{-2} flows further down, while the rest, 30 l m^{-2} is taken up by plants. In case B the proportions of the throughfall water transferred to micropores from the soil surface or from macropores in layers O, E, Bs1, Bs2 and C1 are 18 %, 70 %, 10 %, 2 %, and 0 % respectively (Fig. 12). In case C there is no vertical flow in the micropores, and the corresponding transfers of water to different layers are 19 %, 8 %, 14 %, 20 %, and 2 %. Nearly 30 % of the infiltration flows as a macropore flow straight through the soil profile down to the ground water and omits the chemical reactions in micropores (Fig. 13). The runoff to ground water is 150 l m^{-2} in all cases. In case A there is a quite steady continuous flow to the groundwater, whereas in case C, with only macropore flow, the runoff is formed during the rainy days.

The transpiration losses of different soil layers are almost the same in all cases. Thus a larger proportion of the outflow from the micropores goes to the transpiration stream in case B when compared with case A, and in case C transpiration is the only process transporting water out of the micropores.

4.3 Total Charge of the Soil Solutions

The total positive charge of the soil solution is here considered as the sum of the charges of H^+, Al^{3+}, $Al(OH)^{2+}$, $Al(OH)_2^+$, Ca^{2+}, Mg^{2+} and K^+. Na^+ and NH_4^+ were not included to the sum as the measured values were not available. The total

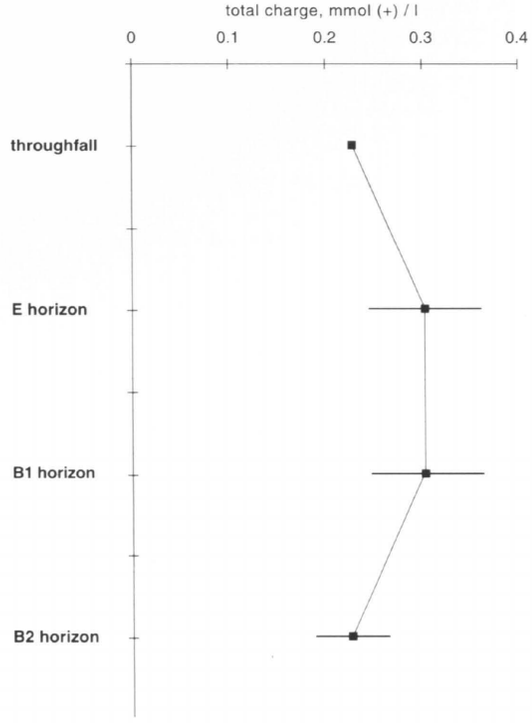

Fig. 14. Total charge (mmol (+) l^{-1}) of cations H^+, $Al(OH)_x^{(3-x)+}$, Ca^{2+}, Mg^{2+}, and K^+ in soil solutions and throughfall. Standard deviation is shown by a line. The numbers of observations are 10, 7 and 13 in the E, Bs1 and Bs2 horizons.

charge is higher in the topmost layers compared to layer Bs2. The average total charge observed increases from throughfall (0.27 $mmol_c$ l^{-1}) to the E and Bs1 horizons (0.32 and 0.31 $mmol_c$ l^{-1} respectively) and decreases in the Bs2 horizon to a smaller value than that in the throughfall (0.23 $mmol_c$ l^{-1}) (Fig. 15). In simulations this vertical gradient is caused by the vertical distribution of the plant water and nutrient uptake, which is closely related to the superficial root distribution, and sulfate adsorption and retention of organic anions with aluminium, which processes take place in the illuvial horizon.The vertical gradient between the layers is most pronounced during the dry periods.

Between the 1st of April and the 15th of May a lot of water from snowmelt flows through the profile and the simulated total charge in the first soil layer follows closely that of the throughfall. The increase in the simulated total positive charge found in the mineral soil layers is caused by the increase in the soil air CO_2 concentration and the following bicarbonate formation. Also the transpiration has a slight increasing effect on the total charge of the simulated soil solution already early in the spring. On the 15th of May, when the first observations of soil solution are available, the simulated total charge of case A (Fig. 14) corresponds well to the observations.

In spring after the 15th of May and in early summer the transpiration increases the total charge, which is nicely shown in both measured and simulated values especially in the E horizon. Dilute summer rains decrease the total charge in soil solution at the end of July and in August, even to values below the initial charge in spring. Also here the simulated solution properties follow closely the scarse measured points. In the Bs1 and Bs2 horizons this effect is not as obvious as in the upper horizons. Unfortunately, the methods of obtaining soil solution for chemical analysis puts limits to the validation of the simulated high peak-concentrations during the dry periods, because water can not be be obtained from the dry soil with suction lysimeters. In September the simulated total charge increases again due to transpiration and the peak in soil air CO_2 concentration. The high total positive charge in precipitation during the autumn months affects also the charge in the soil solution. The decrease in observed total charge on the 27th of November follows the dilute rain events. Here the simulated total charge does not decrease as much as the observed charge although the direction of the change is the same.

The increase in the total charge in the soil horizons is accompanied by a corresponding increase in Cl^--concentration in all horizons and in SO_4^{2-} concentration in the E horizon. In the Bs1 and Bs2 horizons the simulated SO_4^{2-} concentration was regulated by adsorption reaction, which allows only small changes in the soil solution SO_4^{2-} concentration.

The description of the reactions of organic acids (OA) is simple in the model and it was expected to cause the greatest problems in the simulation of the total charge. However, the description of the reactions of OA was quite succesful, as the simulated total charge corresponds well to the measured values in all soil layers.

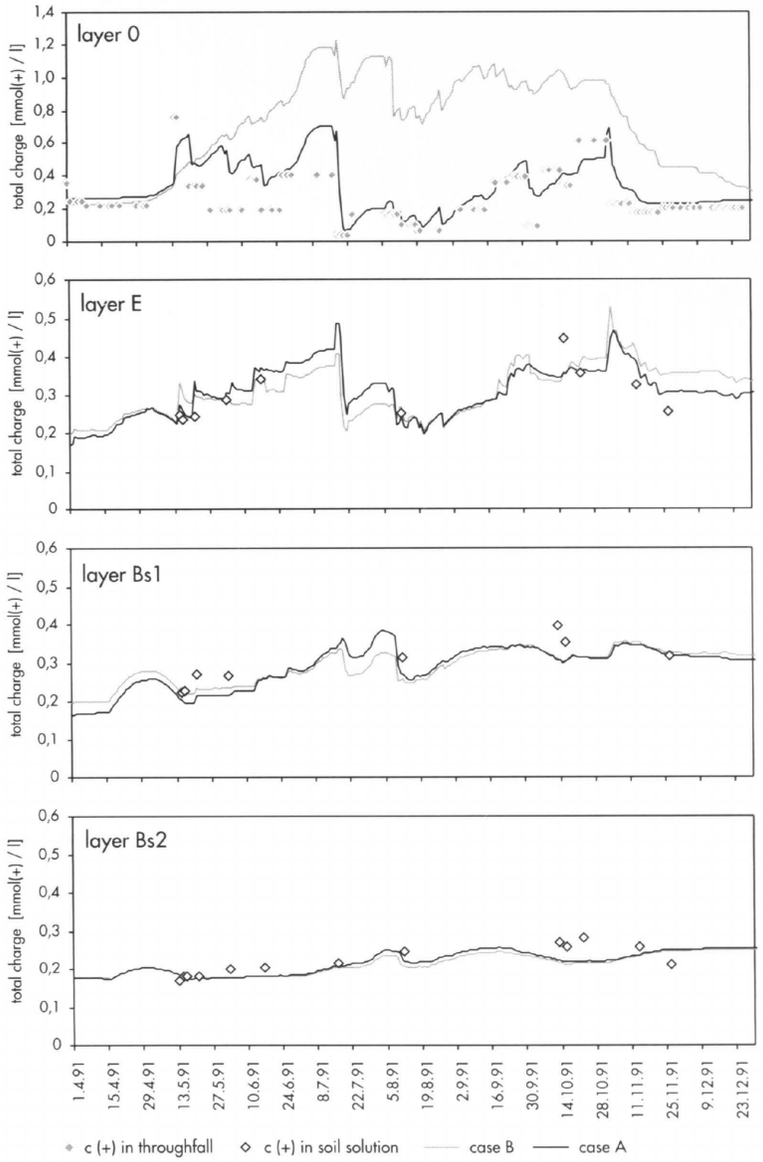

Fig. 15. Total positive charge in simulated cases A and B. The observed total positive charge in throughfall (layer O) and in soil solution of each mineral soil horizon is marked with dots. Na^+ and NH_4^+ are excluded from the total charge.

4.4 Effects of Different Hydrological Descriptions on Simulated Total Charge

Differences in the total charge of soil solution between the three cases can be seen mainly in horizons O and E (Figs. 15 and 16). In case B the dilute summer precipitation does not seep into the dry O horizon to the same extent as in case A. As a result, the total charge and concentrations of each cation rise more in the O horizon in case B than in case A. Concentrations also remain higher

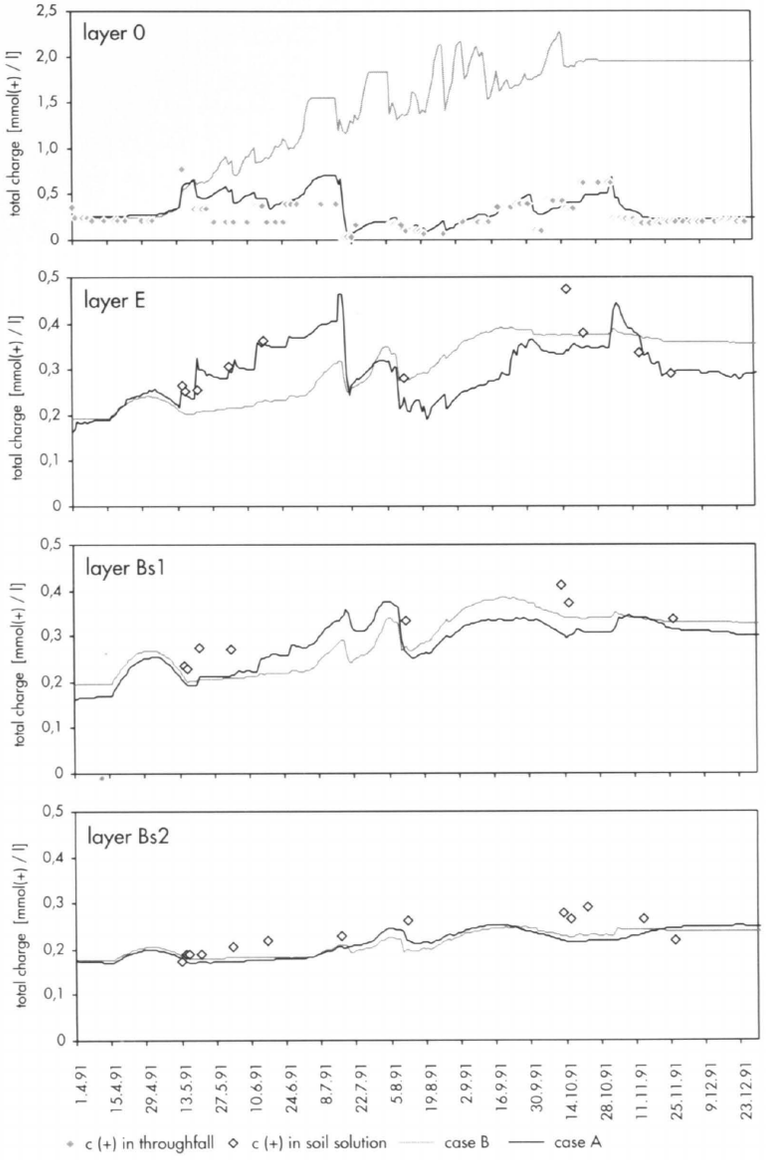

Fig. 16. Total positive charge in cases A and C. Observed total positive charge in throughfall (layer O) and in soil solution of each mineral soil horizon is marked with dots.

until the heavy rains in autumn. However, the concentration changes in the layer E behave in the opposite way. In case B the flow of concentrated solution from the O horizon is small, and in addition a lot of dilute througfall water enters layer E via macropores. In autumn the heavy rains moisten the O and E horizons in case B as well. As a result the hydraulic conductivity and infiltration increase, and concentrations diminish to the same level as in case A. Deeper in soil in the Bs1 and Bs2 horizons the differences between the cases can be seen only as slightly smaller peak

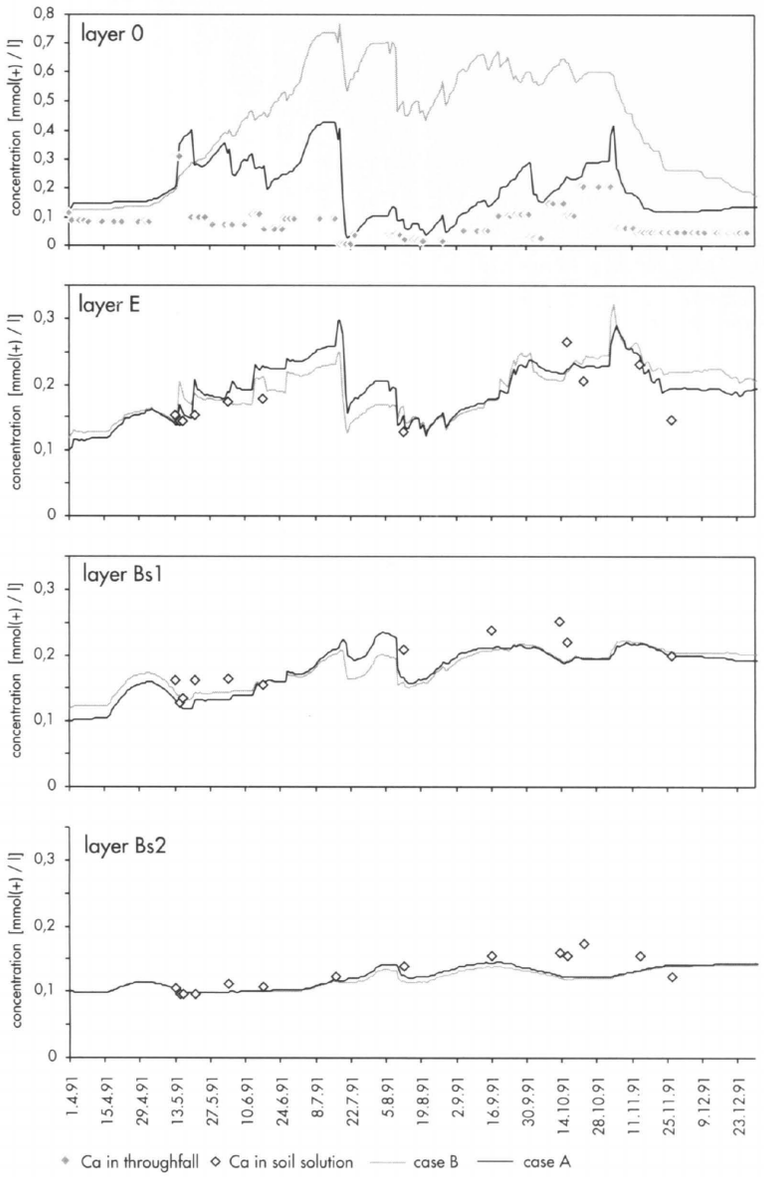

Fig. 17. Solution Ca^{2+} concentration in cases A and B. Observed concentration in throughfall (layer O) and in soil solution of each mineral soil horizon is marked with dots.

concentrations in case B.

In case C the behavior of the concentrations of different ions in soil solution differs from cases A and B in all horizons, the difference being the most prominent in O horizon. Because no vertical flow takes place in the micropores, and new solution flows into micropores only to replace the water taken up by plants, concentrations rise in the O horizon, and are not diluted during the autumn rains. In mineral soil horizons the increase in total charge is not as large as in the O horizon. This is caused by less intensive water uptake in mineral soil and by

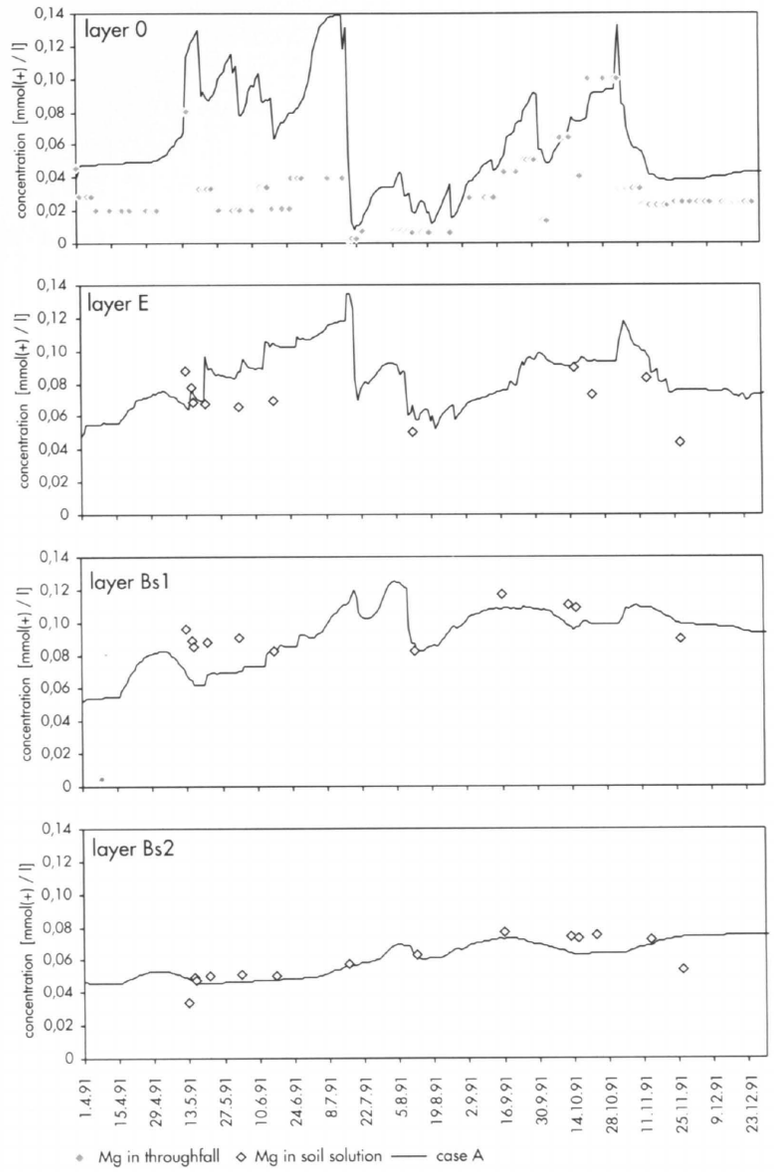

Fig. 18. Solution Mg^{2+} concentration in case A. Observed concentration in throughfall (layer O) and in soil solution of each mineral soil horizon is marked with dots.

sulfate adsorption, which prevents the rise in sulfate concentration. As in other cases, variation in air CO_2 concentration affects the total charge, and brings some fluctuation to the otherwise quite steady increase of concentrations in case C.

Considering the agreement between the observations and simulations, there is not very much difference between cases A and B. Case C does not follow the observations as well as other cases in horizon E, but deeper in soil it produces dynamics and a level of total charge quite similar to the other cases.

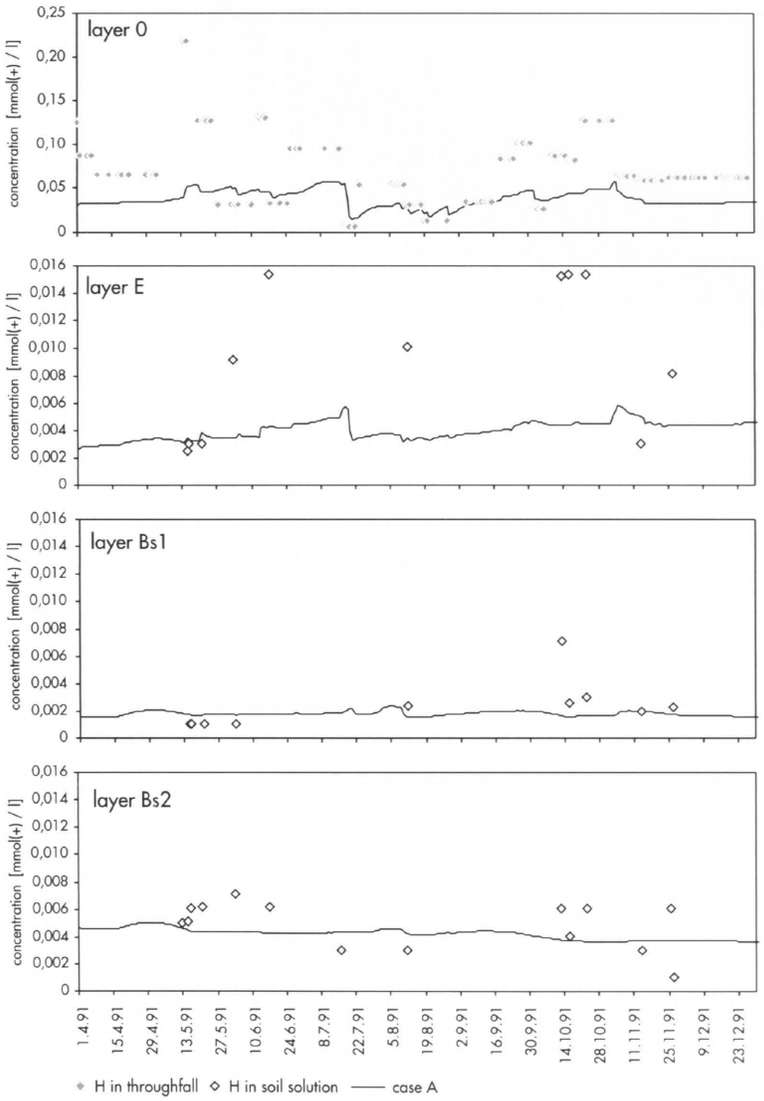

Fig. 19. Solution H^+ concentration in case A. Observed concentration in throughfall (layer O) and in soil solution of each mineral soil horizon is marked with dots.

4.5 Cation Concentrations in the Soil Solutions

4.5.1 Ca *and* Mg

At the first observation date, on the 15th of May, the simulated Ca and Mg concentrations in case A correspond well with the observations (Figs. 17 and 18). Later in the spring and during the summer a lot of fluctuation is seen in the simulated concentrations, in a similar way as was found in the total charge. In the E-horizon the simulated peak concentration of Ca^{2+} was 0.30 $mmol_c\ l^{-1}$ on 16th of July, after which the concentration decreased for two months to a level of 0.13–0.20 $mmol_c\ l^{-1}$ in agreement with the measured concentration. In the Bs1 and Bs2 horizons the measured and simulated Ca^{2+} concentrations are also in good agreement with each other. The behaviour of Mg^{2+} and Ca^{2+} concentrations is similar over the simulated period, and also the simulated and measured Mg^{2+} concentrations follow each other.

The vertical gradients of the measured Ca concentrations are not large, and Ca is the dominant cation in soil solution in all horizons, the concentration of Ca in horizon Bs1 being ten times that of H^+ and Al. Mg also has smaller vertical gradients in soil solution compared to H^+, Al and K.

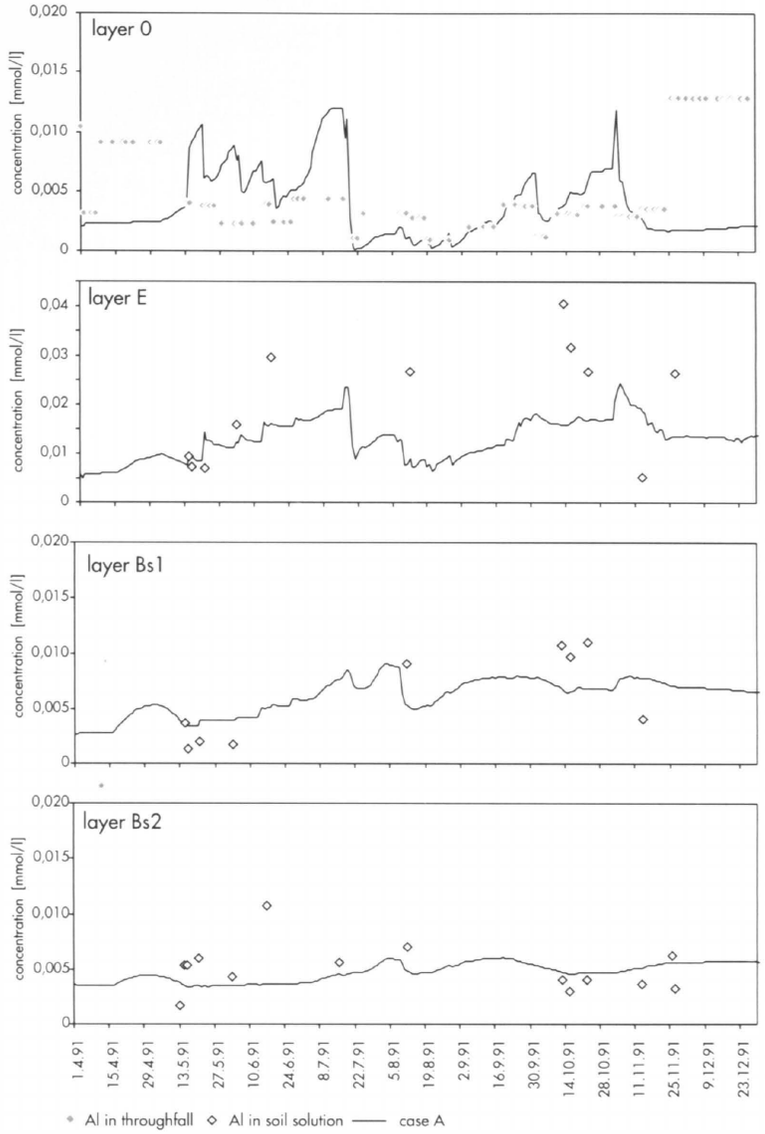

Fig. 20. Solution Al^{3+} concentration in case A. Observed concentration in throughfall (layer O) and in soil solution of each mineral soil horizon is marked with dots.

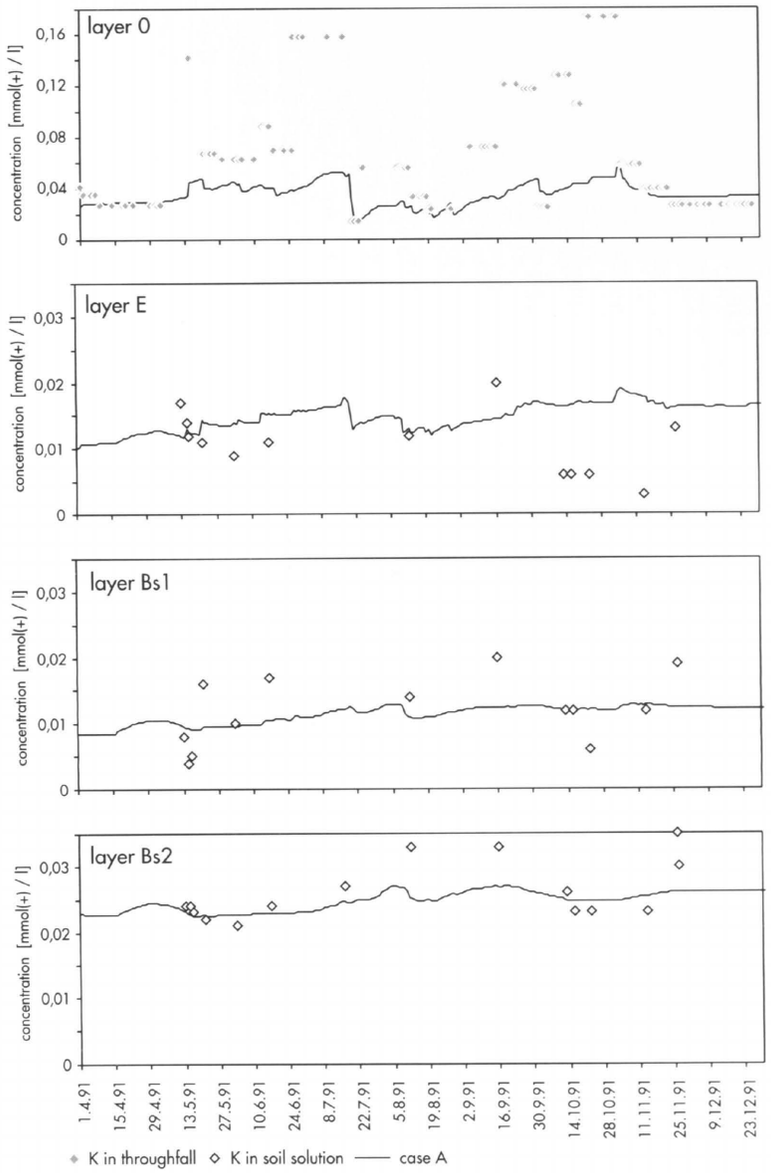

Fig. 21. Solution K^+ concentration in case A. Observed concentration in throughfall (layer O) and in soil solution of each mineral soil horizon is marked with dots.

4.5.2 H^+, Al *and* K

The simulated concentrations of H^+, Al and K are at the same level as those observed, but there is much more fluctuation in the observed than in the simulated concentrations (Figs. 19 to 21). In the B horizons H^+ concentrations are small, only a few per cent of Ca^{2+} concentrations (in $mmol_c\ l^{-1}$), and together with Al about 10 % of Ca^{2+} concentration.

All the simulated cation concentrations in the solution increase at the same time when the ionic strength of the solution increases, which follows from the equilibrium assumptions of the cation exchange and aluminium hydroxide dissolution. However, the higher the charge of the ion is, the greater is the increase of the cation concentration due to the increase in total charge (see also Reuss 1983). As a result, the simulated concentration of Al^{3+} varies most (Fig. 20: Al was assumed to react like Al^{3+} in cation exchange reactions although the average charge of Al was lower) and that of K^+ least (Fig. 21).

The simultaneous rise of all cations can be seen also in the observed soil solution cation concentrations, but not to the same extent as in the simulations. Peaks of only one or two measured ion concentrations indicate that the solution is not in equilibrium with the exchangeable cations. Such non-equilibrium situations seems to be a common phenomena especially for H^+, K and Al in the E and B horizons.

The behaviour of the observed high H^+ concentration in Bs2 is obviously the most problematic to model since the observed H^+ concentration in Bs2 is higher than in the Bs1 horizon, although the base saturation is higher in the Bs2 horizon than the Bs1 horizon. The temporal variation in H^+ concentration in the Bs2 horizon is also large. An obvious explanation for the high H^+ concentration in this horizon as well as large variation in the concentration is that some macropore flow passes the upper horizons and also avoids contact with the exchangeable cations in the Bs2 horizon. As the solution H^+ concentration in throughfall and the O horizon is more than 20 times that of the Bs1 horizon, a small proportion of such solution can cause a large increase in the H^+ concentration. The variation in solution K concentration in the Bs2 horizon also supports such conclusion, as a similar vertical pattern and unexplained variation can be seen for K as for H^+ concentrations.

Although the macropore solution does not react with the exchangeable cations in the model, on a daily basis all simulated soil solution concentrations are in equilibrium with the exchangeable cations. This is, because the macropore solution is assumed to exists in a given soil layer only for a period of some hours, and the transfer of solution from macro to micropores is defined as a rapid process. The differences between the cases in ion concentrations then actually reflect mainly the differences in the dynamics of total charge in micropores created by the different proportion of throughfall water entering each layer.

Altogether the comparison between simulated and observed solution cation concentrations suggests that the flow of solution not in equilibrium with exchangeable cations can be considerable in forest soils. The proportion of such solution may vary with both time and soil depth. Also Hendershot and Chourchesne (1991) observed more week to week variation in measured than in simulated solution cation concentrations, and offered water flow which was not in chemically effective contact with all the soil particle surfaces as an explanation.

4.6 Changes in Exchangeable Cations

A long-term analysis of the changes in the amounts of exchangeable cations was beyond the scope of this article. However, analysis of such changes is one of the aims of the use of model ACIDIC, and thus some aspects concerning the long-term effects of deposition on soil chemistry are considered here.

During the one year simulation period the amount of exchangeable H^+ increased in the O and E horizons, but decreased in the Bs1 and Bs2 horizons (Figs. 22 and 23), although the H^+ concentration in the soil solution of Bs2 horizon was only 10 % of that in throughfall. The net change in the amount of exchangeable H^+ in the soil as a whole was a decrease. An explanation for such result can be found, when it is taken into account that in addition to cation exchange, protons are consumed from the soil solution also in weathering, uptake of NO_3^-, and sulfate adsorption (Fig. 24). The total change ($mmol_c\ l^{-1}$) in sulfate solution concentration due to adsorption in Bs1 and Bs2 horizons is much larger than the average concentration of H^+ in the soil solution of these horizons. As sulfate adsorption is described to produce two moles of OH^- per one mole of SO_4^{2-} adsorbed, H^+ from exchange sites is needed in the model to compensate the OH^- ions produced in the adsorption process. In agreement with this, David et al. (1991) found that input of Na_2SO_4 increased leachate pH in Spodosol columns. Exchangeable H^+ is transferred to potential acidity

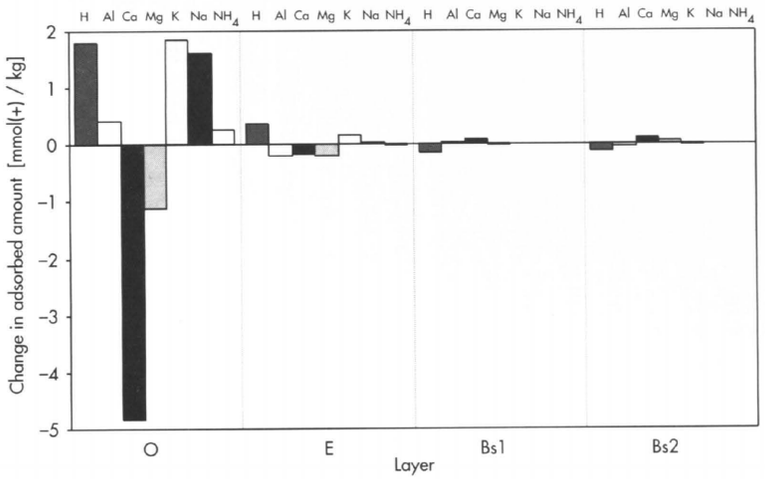

Fig. 22. The changes in the amounts of exchangeable cations (in mmol (+) kg^{-1}) in case A.

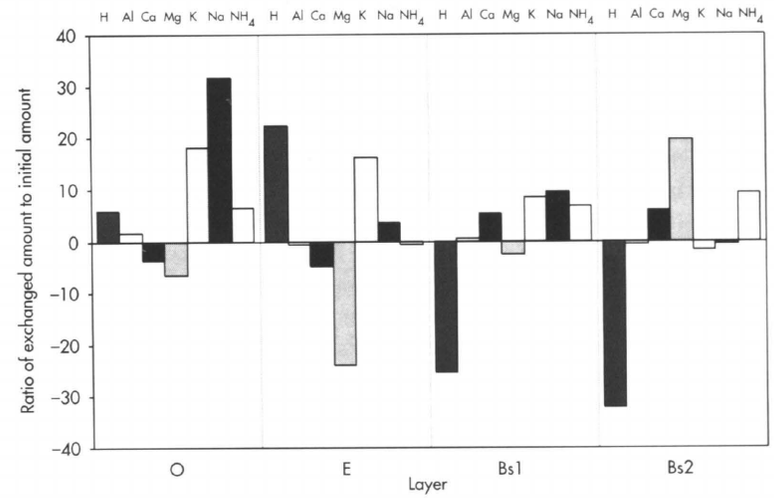

Fig. 23. The relative changes in the amounts of exchangeable cations (% of the initial amount) in case A.

in this process, being stored in adsorbed sulfate. If the solution sulfate concentration decreases due to decreased deposition, the desorption process releases sulfate and protons into the solution.

In the Bs2 horizon cation exchange reactions consume H^+ also from exchange sites, when producing the observed high concentration of H^+ in soil solution. As was discussed earlier, the probable reason for this observed high concentration in soil solution is that lysimeters collect solution which is not in equilibrium with the exchangeable cations and has flowed as preferential flow to horizon Bs2. The simulated changes in exchangeable cation contents in this layer can thus be biased.

Precipitation of $Al(OH)_3$ also affected the simulated concentrations of H^+ and Al, because the simulated H^+ and Al concentrations were in the periods of high total charge at such a level that the solubility of $Al(OH)_3$ was exceeded in horizons E and Bs1. Exchangeable Al was then transferred to $Al(OH)_3$ and at the same time exchangeable H^+ was increased. However, this reaction occurred also in the opposite direction, so that in the autumn all $Al(OH)_3$ was dissolved, consuming solution H^+ and releasing Al into the solution. Thus the reactions of $Al(OH)_3$ had a small effect on H^+ and Al budgets on the annual level (Fig. 24).

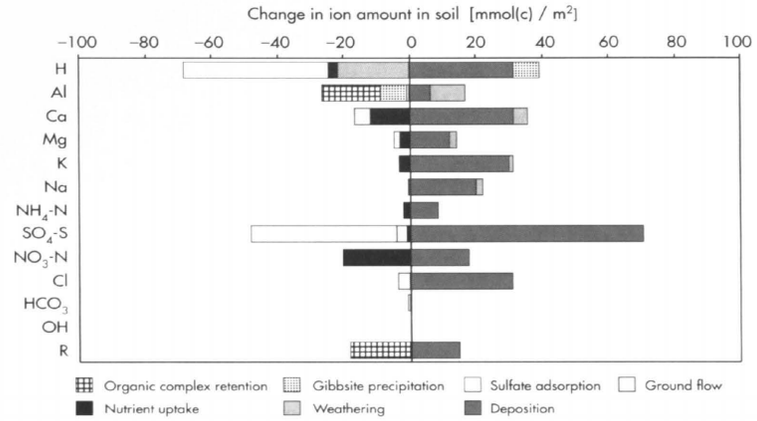

Fig. 24. The inputs and outputs of ions into and from the pool, which includes both exchangeable cations and soluble cations and anions. Case A.

A simultaneous and detailed description of many elements means that any failures in the description of one element are reflected in the simulated behavior of the others as well. Here the deposition of K in throughfall is about 7-fold compared to the open area, while the deposition ratio of Cl^- was only about 2-fold. It is quite obvious that a lot of K observed in the throughfall was actually leached from the needles. Because the assumption used for the nutrient uptake includes only the net uptake of elements, this potassium leaching from needles should not be included to the throughfall in the simulations. When not taken into account, a lot of K was retained on the exchange sites in each horizon and Ca and Mg was leached from the O and E horizons as a result of cation-exchange reactions. Exchangeable Ca and Mg decreased in the O and E horizons and increased in the Bs1 and Bs2 horizons in the simulations. The changes were large to take place during one year.

More base cations were taken up by the trees than was lost in runoff. In case A the uptake corresponds to 70 %, 50 % and over 90 % of the consumption of exchangeable Ca, Mg and K. In case C, with no leaching in the micropores, the changes in exchangeable Ca and Mg are small in the E and Bs1 horizons, and so the processes producing Ca and Mg (infiltration and weathering) were in balance with plant uptake of Ca and Mg. The plant uptake exceeded input in the O horizon, while the exchangeable Ca and Mg increased a little in the Bs2 horizon.

Assuming that the assumptions used for weathering, deposition and net growth are correct, the conclusion from the results of cases A and B concerning changes in the amounts of exchangeable ions, would be that the top soil is still quite far from equilibrium with deposition, and the acidification of the soil continues. The conclusion from case C would be, that the growth slightly acidifies the soil. In case C also a lot of unchanged acid throughfall solution (30 % of throughfall) drained through the macropores into the ground water without any changes in the ion composition. In this kind of system a large acid load would pass through the top soil and affect the deep soil layers and ground water.

4.7 The Use of Model ACIDIC for Analysis of Deposition Effects

ACIDIC has many common features with the other models used for the quantitative analysis of the relations between forest, soil and atmosphere.

According to the review of models made by Tiktak and Van Grinsven (1995), the FORGRO (Mohren 1987), NUCSAM (Kros et al. 1993) and TREGRO (Weinstein et al. 1991) models had a time step of a day or shorter, at least two soil layers, a describtion of unsaturated soil water flow, and a description of dissolution of Al, cation exchange, adsorption of sulfate and formation of bicarbonate. The ILWAS model (Gherini et al. 1985) also has these features. Many other models consider the same processes but have a longer time-step, which could introduce major problems into the analysis of daily hydrological and soil solution ion concentration data.

The description of the water flow in two flow paths, micro and macropores, is an important property of ACIDIC. It is quite evident that a part of the downward water flow omits the chemically most reactive part of the soil, and so models lacking this property fail at least occasionally to produce the concentrations observed in soil solutions. The combined analysis of solution movement and the chemical reactions with the same model gives an additional possibility to analyse the different processes regulating soil chemical characteristics. This possibility is even more useful when the hydrological changes in the forest soils due to the climatic change are to be analysed.

The division of the soil into its main horizons and the use of horizon-specific values for the parameterization of chemical reactions was considered necessary, as the amounts of exchangeable ions as well as soil solution ion compositions were quite different within various soil horizons. Aggregation of soil chemical properties can also lead to an underestimation of acid retention and base cation leaching in podzolic soils (Nissinen 1995). Regarding the solution ion concentrations, the used model structure of ACIDIC was quite successful, even if the connection between the macroflow and the observed peak concentrations of certain elements needs further testing. As Hendershot and Courchesne (1991) pointed out, the reproduction of the temporal pattern of soil solution composition in a profile is "a difficult test of a soil acidification model because processes that cancel each other out when the soil is considered as a whole can have a significant effect in a given horizon".

Sogn (1993), when comparing simulated concentrations of the Magic model and the concentrations in the outflow solution from 40 cm deep lysimeters found that the observed concentrations were far from those simulated, and the only chemical equilibrium which was shown to be valid was that between calcium and magnesium. Sogn concluded that the apparent discrepancy was caused by the consideration of only one homogenous soil layer (the concentrations of exchangeable cations and the exchange parameters were given the values of the 35–40 cm layer), simple flow-routing (all the water reacted with all the soil), and the omission of processes like decomposition.

When comparing the measured and data simulated with ACIDIC on a daily or weekly resolution the description of the decomposition and the nutrient uptake can cause problems. The uptake of nutrients needed for the growth of needles, branches and fine roots was assumed to be equal to the release in the decomposition of litter. Although reasonable assumptions can be done on yearly basis, the within growth period distribution of these two processes can be different. This can be reflected in the total charge of the soil solution and in the concentrations of organic anions, nitrate and cations.

The multi-layer simulation can be seen necessary for the estimations of the ecological effects of soil changes, since the biological activity is consentrated into the O and E horizons. Changes in the nutrient concentrations of these horizons may have a considerable effect on the tree nutrient uptake, even if the changes as a whole are not large when compared to the storage of the exchangeable nutrients in the entire soil profile.

The one-year simulations showed many interesting features of the relations between the simulated processes and solution ion concentrations at different forest soil depths. The hydrology is an important factor affecting on solution chemistry and soil acidification. The description of macropore flow enables the simulation of apparent non-equilibria of cation exchange reactions in bulk soil solution, although equilibria is assumed in micropores. Because the plant water uptake has a large effect on ion concentrations in soil solution, the possibility to model the vertical distribution of roots is important in the analysis of the soil solution chemistry.

5 Conclusions

The hydrological systems in which water was allowed to flow in micro- and macropores (cases A, B) reproduced the observed dynamics in water content in different soil depths quite well. Also in the hydrological system in which water flowed vertically only in macropores (case C), the water content of the soil followed rather closely the observed soil water content. This suggests that whatever transportation route was assumed for the flow of excess water through the system, the soil matrix retained equal amount of water, and the fluctuation in the amount of soil water during the growing season was mainly produced by the temporal combination of transpiration and precipitation.

Even if the total charge was not used in the calibration of the processes that mostly affect it (water and nutrient uptake by plants, retention of organic anion and sulfate adsorption) the simulated vertical and temporal variation in the total charge followed the observations closely. The simulations showed that the temporal variation in the total charge of the soil solution was caused mainly by the variation in the water uptake of plants.

The variation in Ca and Mg concentrations could be simulated in all soil layers. For H^+, Al and K there were much more fluctuation in the observed than in the simulated concentrations, indicating apparent disequilibrium of cation-exchange reactions in the observed soil solutions. For the H^+ and K concentrations having large vertical gradients in soil, a possible explanation for the apparent disequilibrium of the cation exchange is the flow in macropores.

The cation concentrations and total charge differed only slightly between the two hydrological systems described in cases A and B. The simulated total charge in case C differed from that observed, however the case was interesting as it showed one possible way, how two solution phases with very different total positive charge could be formed in soil.

The amount of exchangeable H^+ increased in the O and E horizons and decreased in the Bs1 and Bs2 horizons, the net change in whole soil profile being a decrease. A large part of H^+ decrease in the illuvial B horizon was caused by retention of H^+ in the sulfate adsorption process, which process will again liberate H^+ to solution if the sulfate concentration in percolate decreases.

Based on this application of model ACIDIC, it can be concluded that the model produces soil water amounts and solution ion concentrations which are comparable to the measured values. The combination of a chemical and a hydrological model was shown to be succesfull when the differences between soil layers in solution chemistry were analysed. The model can be used in both hydrological and chemical studies of soils.

Acknowledgements

The co-operation of the researchers of National Board of Waters and Environment in the Rudbäcken catchment is greatly acknowledged. Mikko Jauhiainen kindly provided data of soil water potential and retention characteristics. Professor Pertti Hari encouraged the work, and made some valuable comments on the process descriptions.

References

Addiscott, T.M. 1977. A simple computer model for leaching in structured soils. Journal of Soil Science 28: 554–563.

— 1982. Simulating diffusion within soil aggregates: a simple model for cubic and other regularly-shaped aggregates. Journal of Soil Science 33: 37–45.

— & Wagenet, R.J. 1985. Concepts of solute leaching in soils: a review of modelling approaches. Journal of Soil Science 36: 411–424.

Bartlett, R.J., Ross, D.S. & Magdoff, F.R. 1987. Simple kinetic fractionation of reactive aluminum in soil solutions. Soil Sci. Soc. Am. J. 51: 1479–1482.

Berninger, F. & Hari, P. 1993. Optimal regulation of gas exchange: evidence from field data. Annals of Botany 71: 135–140.

Beven, K. & Germann, P. 1982. Macropores and water flow in soils. Water Resources Research 18: 1311–1325.

Bohn, H.L., McNeal, B.L. & O'Connor, G.A. 1985. Soil chemistry. John Wiley & Sons, New York.

Burns, I.G. 1974. A model for predicting the redistribution of salts applied to fallow soils after excess rainfall or evaporation. Journal of Soil Science 25: 165–178.

Cosby, B.J., Hornberger, G.M., Galloway, J.N. & Wright, R.F. 1985. Modeling the effects of acid deposition: Assessment of a lumped parameter model of soil water and streamwater chemistry. Water Resources Research 21(1): 51–63.

— , Hornberger, G.M., Wright, R.F. & Galloway, J.N. 1986. Modeling the effects of acid deposition: Control of long-term sulfate dynamics by soil sulfate adsorbtion. Water Resources Research 22: 1283–1291.

Darcy, H. 1856. Les fontaines publiques de la Ville de Dijon. Ed. Dalmont, Paris.

David, M.B., Vance, G.F. & Fasth, W.J. 1991. Forest soil response to acid and salt additions of sulfate: II. Aluminum and base cations. Soil Science 151: 208–219.

De Vries, W. & Breeuwsma, A. 1987. The relation between soil acidification and element cycling. Water, Air, and Soil Pollution 35: 293–310.

Duquette, M. & Hendershot, W.H. 1987. Contribution of exchangeable aluminum to cation exchange capacity at low pH. Canadian Journal of Soil Science 67: 175–185.

Falkengren-Grerup, U., Linnermark, N. & Tyler, G. 1987. Changes in acidity and cation pools of South Swedish soils between 1949 and 1985. Chemosphere 16: 2239–2248.

Gaines, G.L. & Thomas, H.C. 1953. Adsorption studies on clay minerals. II. A formulation of thermodynamics of exchange adsorbtion. The Journal of Chemical Physics 21(4): 714–718.

Gapon, E.N. 1933. On the theory of exchange adsorption in soil. J. Gen. Chem. U.S.S.R. 3: 144–152. (In Russian.)

Gherini, S.A., Mok, L., Hudson, R.J.M., Davies, G.F., Chen, C.W. & Goldstein, R.A. 1985. The ILWAS model: Formulation and application. Water, Air and Soil Pollution 26: 425–459.

Handbook of chemistry and physics. A ready-reference book of chemical and physical data. 1948. Hodgman, C.D. (ed.). 30. edition. Chemical Rubber publishing co. 2686 p.

Hendershot, W.H. & Courchesne, F. 1991. Simulation of solution chemistry in an acidic forest soil. Water, Air and Soil Pollution 60: 11–25.

Hyvärinen, A. 1990. Deposition on forest soils – effect of tree canopy on throughfall. In: Kauppi, P., Anttila, P. & Kenttämies, K. (eds.), Acidification in Finland. Springer-Verlag, Berlin Heidelberg. p. 199–216.

James, B.R. & Riha, S.J. 1986. pH buffering in forest soil organic horizons: Relevance to acid precipitation. Journal of Environmental Quality 15: 229–234.

Jauhiainen M. & Nissinen A. 1994. Calibration of the SOIL-model with autumn and summer data of forest soil water tension. In: Kettunen, J., Granlund, K., Paasonen-Kivekäs, M. & Sirviö, H. (eds.), Spatial and temporal variability and interdepencies among hydrological processes. Nordic Hydrological Program NPR, Report 36. p. 17–30. ISBN 951-22-2397-X.

Jenkins, A. & Cosby, B.J. 1989. Modelling surface water acidification using one and two soil layers and simple flow routing. In: Kämäri, J., Braekke, D.F., Jenkins, A., Norton, S.A. & Wright, R.F. (eds.), Regional acidification models. Springer-Verlag. Berlin. p. 253–266.

Johnson, D.W. & Cole, D.W. 1980. Anion mobility in soils: relevance to nutrient transport from forest ecosystems. Environment International 3: 79–90.

Kämäri, J., Seuna, P., Ahlberg, T., Holmberg, M., Kivinen, Y. Lepistö, A., Roos, J. & Soveri, J. 1992. The effect of climate change on the hydrology and material fluxes of forested catchments. Publications of the Academy of Finland 3/1992, p. 101–108.

Korpilahti, E. 1988. Photosyntetic production of Scots pine in the natural environment. Acta Forestalia Fennica 202. 71 p.

Kros, J., De Vries, W., Janssen, P.H.M. & Bak, C.I. 1993. The uncertainty in forecasting trends of forest soil acidification. Water, Air and Soil Pollution 66: 29–58.

Lindsay, W.L. 1979. Chemical equilibria in soils. Wiley-Interscience, New York.

Liski, J. & Pumpanen, J. 1994. Spatial and temporal variation in concentration of dissolved organic carbon. In: Jauhiainen, M. (ed.), The national SILMU meeting, Aulanko, Finland, March 23–24, 1994. Posters presented on projects of the Department of Forest Ecology. University of Helsinki, Department of Forest Ecology, Publications 10, p. 22–25.

Lundström, U. 1993. The role of organic acids in the soil solution chemistry of a podzolized soil. Journal of Soil Science 44: 121–133.

Luxmoore, R.J., Jardine, P.M., Wilson, G.V., Jones, J.R. & Zelagny, L.W. 1990. Physical and chemical controls of preferred path flow through a forested hillslope. Geoderma 46: 139–154.

Magnusson, T. 1992. Temporal and spatial variation of the soil atmosphere in forest soils of northern Sweden. Swedish University of Agricultural Sciences, Department of Forest Site Research, Stencil 22. ISSN 0280-9168.

Majdi, H. & Persson, H. 1993. Spatial distribution of fine roots, rhizosphere and bulk soil chemistry in an acidified Picea abies stand. Scandinavian Journal of Forest Research 8: 147–155.

Mecke, M. 1994. Carbon in boreal coniferous forest soil: Hydraulic conductivity in podzolized soils. In: Jauhiainen, M. (ed.), The national SILMU meeting, Aulanko, Finland, March 23–24, 1994. Posters presented on projects of the Department of Forest Ecology. University of Helsinki, Department of Forest Ecology, Publications 10, p. 26–29.

—, Ilvesniemi, H. & Westman, C.J. 1999. Estimation of soil water retention capacity by structural, textural and pedogenic parameters in podzolic soils. Manuscript.

Mengel, K. & Kirkby, E.A. 1987. Principles of plant nutrition. International Potash Institute, Worblaufen-Bern.

Mohren, G.M.J. 1987. Simulation of forest growth, applied to Douglas fir stands in the Netherlands. Ph.D. thesis, Agricultural University, Wageningen.

Mualem, Y. 1976. A new model for predicting the hydraulic conductivity of unsaturated media. Water Resour. Res. 12(3): 513–522.

Neal, C. & Robson, A.J. 1997. Integrating variations of soil-adsorbed cations into a cation exchange model. Sci. Total Environ. 199: 277–292.

Nielsen, D.R., Van Genuchten, M.T. & Biggar, J.W. 1986. Water flow and solute transport processes in unsaturated zone. Water Resour. Res. 22(9): 89S–108S.

Nissinen, A. 1995. Simulated effects of acid deposition on podzolic soils: consequences of process and parameter aggregation. Water Air and Soil Pollution 85: 1107–1112.

— & Ilvesniemi, H. 1990. Effects of acid deposition on exchangeable cations, acidity and aluminium solubility in forest soils and soil solution. In: Kauppi, P., Anttila, P. & Kenttämies, K. (eds.), Acidification in Finland. Springer-Verlag, Berlin Heidelberg. p. 287–304.

— , Ilvesniemi, H. & Tanskanen, N. 1998. Apparent cation-exchange equilibria in podzolic forest soils. European Journal of Soil Science 49: 121–132.

Reuss, J.O. 1983. Implications of the calcium-aluminium exchange system for the effect of acid precipitation on soils. Journal of Environmental Quality 12: 591–595.

Richards, L.A. 1931. Capillary conduction of liquids in porous mediums. Physics 1: 318–333.

Sogn, T.A. 1993. A test of chemical equilibrium equations and assumptions commonly used in soil-oriented charge balance models for soil and freshwater acidification. Ecological Modelling 70: 221–238.

Sverdrup, H. & Warfvinge, P. 1993. Calculating field weathering rates using a mechanistic geochemical model PROFILE. Applied Geochemistry 8: 273–283.

Tamm, C.O. & Hallbäcken, L. 1988. Changes in soil acidity in two forest areas with different acid deposition: 1929s to 1980s. Ambio 17(1): 56–61.

Terkeltroub, R.W. & Babcock, K.L. 1971. A simple method for predicting salt movement through soil. Soil Science 111: 182–187.

Tiktak, A. & Van Grinsven, H.J.M. 1995. Review of sixteen forest-soil-atmosphere models. Ecological Modelling 83: 35–53.

Ulrich, B. 1983. Soil acidity and its relations to acid deposition. In: Ulrich, B. & Pankrath, J. (eds.), Effects of accumulation of air pollutants in forest ecosystems. D. Reidel Publishing Company, Dordrecht. p. 127–146.

Vakkilainen, P. 1986. Haihdunta. In: Mustonen, S. (ed.), Sovellettu hydrologia. Vesiyhdistys ry., Helsinki. p. 64–81. (in Finnish.)

Van Genuchten, M.T. 1980. A closed-form equation for predicting the hydraulic conductivity of unsaturated soils. Soil Sci. Soc. Am. J. 44(5): 892–898.

Warfvinge, P., Falkengren-Grerup, U. & Sverdrup, H. 1992a. Modeling long-term base supply to acidifed forest stands. Environmental Pollution 80: 209–221.

— , Holmberg, M., Posch, M. & Wright, R.F. 1992b. The use of dynamic models to set target loads. Ambio 21: 369–376.

Weinstein, D.A., Beloin, R.M. & Yanai, R.D. 1991. Modelling changes in red spruce carbon balance in response to interacting ozone and nutrient stresses. Tree Physiology 9: 127–146.

Total of 57 references

Submission of Manuscripts Manuscripts should be submitted in triplicate to Acta Forestalia Fennica, Unioninkatu 40 A, FIN-00170 Helsinki, Finland. Detailed instructions to authors have last been printed in Acta Forestalia Fennica 244, are available from the editorial office, and can be found on Acta's WWW pages at http://www.metla.fi/publish/acta/

Publication Schedule Acta Forestalia Fennica is published intermittently, 3 to 6 numbers per year.

Subscriptions and Exchange Subscriptions and orders for back issues should be addressed to Academic Bookstore, Subscription Services, P.O. Box 108, FIN-00101 Helsinki, Finland, Phone +358 9 121 4322, Fax +358 9 121 4435. Subscription price for 1999 is 70 FIM per issue. Exchange inquiries should be addressed to the Finnish Society of Forest Science, Unioninkatu 40 A, FIN-00170 Helsinki, Finland, Phone +358 9 8570 5235, Fax +358 9 8570 5 677, E-mail sms@helsinki.fi

Statement of Publishers Acta Forestalia Fennica has been published since 1913 by the Finnish Society of Forest Science. In 1989 Acta Forestalia Fennica was merged with Communicationes Instituti Forestalis Fenniae, started in 1919 by the Finnish Forest Research Institute. In the merger, the Society and Forest Research Institute became co-publishers of Acta Forestalia Fennica. The Finnish Society of Forest Science is a nonprofit organization founded in 1909 to promote forest research. The Finnish Forest Research Institute, founded in 1917, is a research organization financed by the Ministry of Agriculture and Forestry.

Abstracting Articles in Acta Forestalia Fennica are abstracted and indexed in Agrindex, Biological Abstracts, Current Advances in Ecological Sciences, Current Advances in Plant Sciences, Ecological Abstracts, Forest Products Journal, Forestry Abstracts, International Bibliography of Periodical Literature, Life Sciences Collection.

ACTA FORESTALIA FENNICA
The Finnish Society of Forest Science
The Finnish Forest Research Institute

252 **Pekka Ripatti:** Factors affecting partitioning of private forest holdings in Finland. A logit analysis.

253 **Vesa Kaarakka:** Management of bushland vegetation using rainwater harvesting in eastern Kenya.

254 **Pertti Hari, Juhan Ross and Marja Mecke (eds.):** Production process of Scots pine; geographical variation and models.

255 **Euan G. Mason and A. Graham D. Whyte:** Modelling initial survival and growth of radiata pine in New Zealand.

256 **Juha Nurmi:** Heating values of mature trees.

257 **Timo Hartikainen:** Late-industrial sawmill customers. The concept of industrial operating mode and its testing in secondary wood processing industry.

258 **Jari Varjo:** Change detection and controlling forest information using multi-temporal Landsat TM imagery.

259 **Jori Uusitalo:** Pre-harvest measurement of pine stands for sawing production planning.

260 **Wending Huang:** Productive coexistence and gain in agroforestry systems.

261 **Johanne M.G. Morasse:** Estimation of cutting volume with three inventory methods for harvest planning in Canadian boreal forests

262 **Timo Kareinen, Ari Nissinen and Hannu Ilvesniemi:** Analysis of forest soil chemistry and hydrology with a dynamic model ACIDIC.

ISBN 951-40-1663-7
ISSN 0001-5636

Cover: Jarmo Koivunen

ACTA FORESTALIA FENNICA 262 • 1998